Calhoun: The NPS Institutional Archive

DSpace Repository

Theses and Dissertations | 1. Thesis and Dissertation Collection, all items

2016

CFD analysis of the SBXC Glider airframe

Garcia, Alejandro Aguilar

Monterey, California: Naval Postgraduate School

http://hdl.handle.net/10945/49466

Copyright is reserved by the copyright owner.

Downloaded from NPS Archive: Calhoun

http://www.nps.edu/library

Calhoun is the Naval Postgraduate School's public access digital repository for research materials and institutional publications created by the NPS community. Calhoun is named for Professor of Mathematics Guy K. Calhoun, NPS's first appointed -- and published -- scholarly author.

Dudley Knox Library / Naval Postgraduate School
411 Dyer Road / 1 University Circle
Monterey, California USA 93943

NAVAL POSTGRADUATE SCHOOL

MONTEREY, CALIFORNIA

THESIS

CFD ANALYSIS OF THE SBXC GLIDER AIRFRAME

by

Alejandro Garcia Aguilar

June 2016

Thesis Advisor:	Kevin D. Jones
Co-Advisor:	Vladimir N. Dobrokhodov
Second Reader:	Isaac Kaminer

Approved for public release; distribution is unlimited

THIS PAGE INTENTIONALLY LEFT BLANK

REPORT DOCUMENTATION PAGE			Form Approved OMB No. 0704–0188
Public reporting burden for this collection of information is estimated to average 1 hour per response, including the time for reviewing instruction, searching existing data sources, gathering and maintaining the data needed, and completing and reviewing the collection of information. Send comments regarding this burden estimate or any other aspect of this collection of information, including suggestions for reducing this burden, to Washington headquarters Services, Directorate for Information Operations and Reports, 1215 Jefferson Davis Highway, Suite 1204, Arlington, VA 22202-4302, and to the Office of Management and Budget, Paperwork Reduction Project (0704-0188) Washington, DC 20503.			
1. AGENCY USE ONLY ***(Leave blank)***	**2. REPORT DATE** June 2016	**3. REPORT TYPE AND DATES COVERED** Master's thesis	
4. TITLE AND SUBTITLE CFD ANALYSIS OF THE SBXC GLIDER AIRFRAME			**5. FUNDING NUMBERS**
6. AUTHOR(S) Alejandro Garcia Aguilar			
7. PERFORMING ORGANIZATION NAME(S) AND ADDRESS(ES) Naval Postgraduate School Monterey, CA 93943-5000			**8. PERFORMING ORGANIZATION REPORT NUMBER**
9. SPONSORING /MONITORING AGENCY NAME(S) AND ADDRESS(ES) N/A			**10. SPONSORING / MONITORING AGENCY REPORT NUMBER**
11. SUPPLEMENTARY NOTES The views expressed in this thesis are those of the author and do not reflect the official policy or position of the Department of Defense or the U.S. Government. IRB Protocol number____N/A____.			
12a. DISTRIBUTION / AVAILABILITY STATEMENT Approved for public release; distribution is unlimited			**12b. DISTRIBUTION CODE**

13. ABSTRACT (maximum 200 words)

The research of this thesis develops and implements a computational model of the SBXC Glider utilized in the Tactical Long-Endurance Unmanned Aerial System (TaLEUAS) project in order to simulate the aerodynamic performance of the airframe and compare it with real flight data. The broader goals are first, to provide a methodology for simulating a glider design with the intention to develop an optimization process or to evaluate a new design using computational tools; and second, to allow students to follow an easy process in which to undertake similar aerodynamic analyses. The fluid behavior is studied using computer software such as Ansys CFX, which is based mathematically on finite element methods.

To validate and verify the methodology developed, a mathematical comparison was made with the previous research data obtaining a similar region for best flying behavior. Recommendations are given to increase the accuracy of the flying performance for velocities greater than 15 m/s.

14. SUBJECT TERMS finite element method, computational fluid dynamics, Y Plus, mesh element quality, aerodynamic data, fluid domain, Solidworks/ANSYS, 3D modeling and simulation			**15. NUMBER OF PAGES** 103
			16. PRICE CODE
17. SECURITY CLASSIFICATION OF REPORT Unclassified	**18. SECURITY CLASSIFICATION OF THIS PAGE** Unclassified	**19. SECURITY CLASSIFICATION OF ABSTRACT** Unclassified	**20. LIMITATION OF ABSTRACT** UU

NSN 7540–01-280-5500 Standard Form 298 (Rev. 2–89)
Prescribed by ANSI Std. 239–18

THIS PAGE INTENTIONALLY LEFT BLANK

Approved for public release; distribution is unlimited

CFD ANALYSIS OF THE SBXC GLIDER AIRFRAME

Alejandro Garcia Aguilar
Lieutenant Junior Grade, Mexican Navy
B.S., School of Engineering of the Mexican Navy

Submitted in partial fulfillment of the
requirements for the degrees of

MECHANICAL ENGINEER

and

MASTER OF SCIENCE IN MECHANICAL ENGINEERING

from the

NAVAL POSTGRADUATE SCHOOL
June 2016

Approved by: Kevin D. Jones
Thesis Advisor

Vladimir N. Dobrokhodov
Co-Advisor

Isaac Kaminer
Second Reader

Garth V. Hobson
Chair, Department of Mechanical and Aerospace Engineering

THIS PAGE INTENTIONALLY LEFT BLANK

ABSTRACT

The research of this thesis develops and implements a computational model of the SBXC Glider utilized in the tactical long-endurance unmanned aerial system (TaLEUAS) project in order to simulate the aerodynamic performance of the airframe and compare it with real flight data. The broader goals are first, to provide a methodology for simulating a glider design with the intention to develop an optimization process or to evaluate a new design using computational tools; and second, to allow students to follow an easy process in which to undertake similar aerodynamic analyses. The fluid behavior is studied using computer software such as Ansys CFX, which is based mathematically on finite element methods.

To validate and verify the methodology developed, a mathematical comparison was made with the previous research data obtaining a similar region for best flying behavior. Recommendations are given to increase the accuracy of the flying performance for velocities greater than 15 m/s.

THIS PAGE INTENTIONALLY LEFT BLANK

TABLE OF CONTENTS

I. INTRODUCTION 1
A. MOTIVATION 2
B. TaLEUAS 2
1. NPS Students' Progress 4
C. THESIS OBJECTIVES 7
D. FORMULATION OF THE PROBLEM 8
E. BACKGROUND AND PREVIOUS RESEARCH 8
1. FEM and CFD 8
2. Performance Testing of RNR's SBXC Using GPS 10
3. Performance Testing of RNR's SBXC Using Piccolo-Autopilot 12
4. CFD UAV Analysis Background 14
F. THESIS OUTLINE 16

II. MODELING THE GLIDER AND THE FLUID DOMAIN 17
A. INTRODUCTION TO SBXC GLIDER DESIGN 17
B. MODELING GENERATION 18
1. Sketch Picture and Airfoil Coordinates Generator Software 18
2. Generation of Fluid Domain 20
3. Import the Fluid Domain into ANSYS CFX 22

III. PRE-PROCESSING 23
A. OVERVIEW 23
B. MESHING 23
1. Meshing Advance Size Function Available for Fluids Dynamics 24
2. Inflation Techniques for Fluids Dynamics 26
3. Mesh Quality 27
C. BOUNDARY CONDITIONS 29
1. Default Domain 29
2. Inlet, Outlet, Wall, Opening 30
D. SOLVER CONTROL 31
E. HAMMING 32
1. Hamming Configuration 33
2. Hamming-ANSYS CFX Communication Link 33

IV. POST-PROCESSING 37
A. OVERVIEW 37
B. CONVERGENCE CRITERION 37
1. Common Errors during the CFD Process 39
2. User Error 40
3. Residual Error 41
C. YPLUS VALUE 41
D. PRESSURE AND VELOCITY CONTOURS 45
E. DERIVED DATA 48
1. Coefficient of Lift and Drag 50
2. Sink Polar 51

V. RESULTS AND COMPARISON WITH REAL FLIGHT DATA 57

VI. CONCLUSIONS AND FUTURE WORK 61
A. CONCLUSIONS 61
B. FUTURE WORK 62

Appendix. Solidworks-ANSYS-Hamming Simulation Process Gouge for Aerodynamics Analysis of the SBXC Wing 63

LIST OF REFERENCES 79

INITIAL DISTRIBUTION LIST 83

LIST OF FIGURES

Figure 1. Comparison between Real SBXC Glider (top) and SBXC Computer Model (bottom). 2

Figure 2. Mission Airspace Cone Boundary during Allen's Simulation. Source: [1]. 3

Figure 3. Simulation of Cooperating UAVs. Source: [5]. 5

Figure 4. Tracking of Thermal during Climb. Source: [7]. 6

Figure 5. Cooperative Flight of Three Gliders. Source: [8]. 6

Figure 6. Identification of Nodes and Elements in a Two Dimensional Mesh. 9

Figure 7. Ellias Sink Rate Plot. Source: [11]. 11

Figure 8. SBXC Sink Polar. Source: [12]. 13

Figure 9. Comparison of Wing with various Winglets. Source: [15]. 14

Figure 10. Flow Development around the Fuselage. Source: [17]. 15

Figure 11. S2048 Airfoil Behavior in Different Reynolds Numbers. Source: [18] 17

Figure 12. Picture Sketch Technique Applied to the SBXC Fuselage. 18

Figure 13. Left Wing of the SBXC Glider created with Professor Jones's Software. 20

Figure 14. Assembly of the SBXC Glider with the Fluid Domain. 21

Figure 15. Final State of the Fluid Domain. 22

Figure 16. Meshing Application Interface. Source: [20]. 24

Figure 17. Size Functions Behavior. Adapted from [21]. 26

Figure 18. First Layer Inflation Applied to the SBXC Wing. 27

Figure 19. Last Aspect Ratio Inflation Applied to the SBXC Wing. 27

Figure 20. Section of the SBXC Fluid Domain after the Meshing Process. 28

Figure 21. Element Quality Graph for the SBXC Fluid Domain. 28

Figure 22. Boundaries Conditions for the SBXC Fluid Domain. 31

Figure 23. Solver Control–Command Editor. 32

Figure 24. Command List to open CFX-Pre in Hamming. 34

Figure 25. Creation of a Definition File in Hamming Environment. 35

Figure 26. Residual Momentum and Mass Monitor of the SBXC Glider at 12 m/s with 3 Degrees AoA Matching with the Residual Target. Based on [14]. 38

Figure 27. Residual Tangential Force in X Direction Monitor of the SBXC Glider at 12 m/s with 4.59 Degrees AoA for 200 Iterations. 38

Figure 28. Consistency and Stability Comparison between Two Different Quality Meshes for the SBXC Wing at 12 m/s at 3 Degrees AoA at 100 Iterations. 39

Figure 29. Mesh Failure Due to Bad Geometry Construction of the SBXC Airframe. 40

Figure 30. Sig Handler Error Due to a Wrong Selection of Partition Method. 40

Figure 31. Boundary Layer Separation Over an Airfoil. Source: [25]. 42

Figure 32. Development of the Boundary Layer for Flow Over a Flat Plate and the Different Flow Regimes. Source [26]. 42

Figure 33. y^+ Range between Flow Regimes. Source: [24]..... 43

Figure 34. Comparison of y^+ between Two Different Values of First Layer Thickness for the SBXC Glider Fluid Domain. 44

Figure 35. Pressure Body Contour of the SBXC Glider at 12 m/s at 4.59 Degrees AoA. 45

Figure 36. Plane Pressure Contour of the SBXC Glider at 12m/s with 4.59 Degrees AoA. 46

Figure 37. Boundary Layer Thickness for the SBXC Glider at 12 m/s with 4.59 Degrees AoA. 46

Figure 38. Velocity Analysis of the SBXC at 12 m/s with 4.59 Degrees AoA. 47

Figure 39. Wall Shear around a SBXC Wing Section. 48

Figure 40. Free Body Diagram for the SBXC Equilibrium Analysis..... 49

Figure 41. Linear Approximation Technique at 15 m/s for the SBXC Glider. 50

Figure 42. Cl and Cd Trend Lines for the SBXC Glider at 18 m/s..... 51

Figure 43. GA Relationship for the SBXC Model. 52

Figure 44. L/D Performance of the SBXC Glider Using CFD Technique. 53

Figure 45. Sink Polar for the SBXC Glider Using CFX. 54

Figure 46. L/D Performance of the SBXC Glider Using Real Data Flight and CFX Techniques. 57

Figure 47. Sink Polar Comparison between Real Flight Data and CFX Analysis. 58

Figure 48. SBXC Mid Wing Section Structural View. Airfoil and Guide Curve Process. 64

Figure 49. Solid SBXC Wing after the Loft Instruction. 65

Figure 50. Creation of a Reference Plane in the Root of the Wing. 65

Figure 51. Extrusion Created with the Wing Inside. Both Solids Are Merged. 66

Figure 52. Wing Fluid Domain. 66

Figure 53. Import a Parasolid File to ANSYS CFX. 67

Figure 54. SBXC Fluid Domain, Named Selection Process. 68

Figure 55. Mesh Generated for the SBXC Wing. 69

Figure 56. Good Mesh Quality for the SBXC Wing. 69

Figure 57. Boundary Conditions Applied to the SBXC Wing Fluid Domain. ... 71

Figure 58. Hamming Communication Script. 73

Figure 59. MobaXterm Window with Script and CFX Files. 74

Figure 60. Velocity Profile Using Plane Instruction. 75

Figure 61. Pressure Profile Using Plane Instruction. 76

Figure 62. Yplus Body Profile Using Contours Instruction. 76

Figure 63. Pressure Body Profile Using Contours Instruction. 77

LIST OF TABLES

Table 1. Ellias SBXC Performance Test. Source: [11]. 11

Table 2. Raw Data and Computed Parameters from Flight Testing. Source: [12]. 13

Table 3. Airfoil Coordinates Generator Inputs Data. 19

Table 4. SBXC Dimensions. 21

Table 5. ANSYS Size Functions Characteristics. 25

Table 6. ANSYS Inflation Techniques. Adapted from [21]. 26

Table 7. Element Quality Statistics Table. 29

Table 8. Default Domain Configuration for SBXC Airframe Analysis. 29

Table 9. Solver Control Configuration for the SBXC Analysis. 31

Table 10. Hamming Basic Commands. 34

Table 11. Range of Velocities Analyzed for the SBXC Glider. 49

Table 12. Cl and Cd Table for the Velocities Analyzed in the SBXC Glider Computer Model. 51

Table 13. L/D and Velocities Components. 53

Table 14. SBXC-CFD Min and Best L/D Velocities Values and Derived Data. 55

Table 15. Comparison Data between Real Flight and CFX Data. 59

Table 16. Best L/D for All the Methods Using the Free Stream Velocity without Fitting a Polynomial. 60

THIS PAGE INTENTIONALLY LEFT BLANK

LIST OF ACRONYMS AND ABBREVIATIONS

2D	two dimensions
3D	three dimensions
3Dof	three degrees of freedom
6Dof	six degrees of freedom
AoA	Angle of attack
BC	Boundary Conditions
CAD	Computer-Aided design
CAE	Computer-Aided Engineering
Cd	coefficient of drag
CFD	Computational Fluid Dynamics
Cl	coefficient of lift
D	drag force
FEA	Finite Element Analysis
FEM	Finite Element Method
GA	Gliding Angle
GPS	Global Positioning System
L	lift force
MALE UAV	medium altitude long endurance unmanned aerial vehicle
MBD	Multibody Dynamics
NPS	Naval Postgraduate School
TaLEUAS	Tactical Long-Endurance Unmanned Aerial System
UAS	Unmanned Aerial System
UAV	Unmanned Aerial Vehicle
V_h	horizontal velocity
V_s	sink velocity
W	Weight

THIS PAGE INTENTIONALLY LEFT BLANK

ACKNOWLEDGMENTS

I want to thank God for His blessing in all moments and for the opportunity to walk on the path of truth and knowledge.

My eternal thankfulness is dedicated to the love of my life, Stephany, for showing me the most beautiful feeling in the world, a feeling that helps me to face every challenge present in my life.

I am forever grateful to my parents and siblings for being there for me all the time. Their unconditional support and love have made me the person of good will that I am now.

I would like to thank the Mexican Navy for the opportunity to be an NPS student, particularly to CDR Mariano Lizarraga, CDR Miguel Alvarado, and LT Nahum Camacho for their advice at the beginning of my military career and for revealing to me the world of unmanned systems.

The accomplishment of this research is due to the advice, knowledge, and patience of Doctors Kevin Jones, Vladimir Dobrokhodov, Isaac Kaminer, and Young Kwon. Without their unlimited help, this project would not be completed. I will always be thankful to them for being my wise guides.

THIS PAGE INTENTIONALLY LEFT BLANK

I. INTRODUCTION

The object of this thesis is to use modern commercial computational fluid dynamic (CFD) tools to estimate the glide performance of the SBXC airframe, with comparisons to existing experimental data. The intention of this research is to develop a simulation approach accurate enough to be used as an estimator of the performance of future airframes prior to manufacturing. The results obtained in the simulation will help reduce manufacturing costs and expedite airframe development.

The SBXC airplane is currently utilized as the flight platform in the Naval Postgraduate School (NPS) tactical long-endurance unmanned aerial system (TaLEUAS) project. The primary goal of the project is to develop an unmanned aerial system (UAS) capable of accomplishing missions for extremely long periods of time using two sources of environmental energy: photovoltaic (solar) and convective lift (thermal).

Computer-aided design (CAD), along with CFD software, are invaluable assets for engineering study, especially in fluid dynamics. Software like ANSYS-CFX use a technique based on finite element methods (FEM), which can be defined as the technique of mathematically solving a complex domain by dividing it into small elements to create subdomains.

This research was developed using ANSYS-CFX software. CFX is considered a CFD tool capable of solving complex domains by solving Navier-Stokes equations that describe the fluid physics. It includes a user-friendly GUI (graphic user interface) to help the user set up complex geometries, mesh, apply initial/boundary conditions, solve and finally post-process and view results. In Figure 1, the comparison between the real SBXC glider with the computer model used to develop the project can be observed:

Figure 1. Comparison between Real SBXC Glider (top) and SBXC Computer Model (bottom).

A. MOTIVATION

The primary goal of this thesis is to develop a methodology that allows aeronautic engineers and students to undertake aerodynamic fluid tests, using commercial CFD tools with the objective to implement an optimization process or develop a completely new aerodynamic design based on the basic interpretation of the graphic and mathematical results obtained in the simulation.

B. TaLEUAS

TaLEUAS is a project initiated at NPS with the objective of having an Unmanned Aerial Vehicle (UAV) capable of accomplishing intelligence and surveillance operations by flying 24/7 using solar energy, thermal air currents, and stored battery energy.

The gliders use convective lift as one of the natural energy sources. Michael J. Allen developed an analysis of how an UAV can increase the endurance over a target location based on a three degrees of freedom (3DoF) simulation to determine the thermal performance during the four seasons of the year in Desert Rock, Nevada [1]. A mathematical model for the thermals used in the simulation was developed using surface radiation and rawinsonde balloon measurements of the area. The Archimedes spiral was chosen as the flight

pattern for the UAV to avoid crossing the same point twice for a pre-determined circular area (Figure 2):

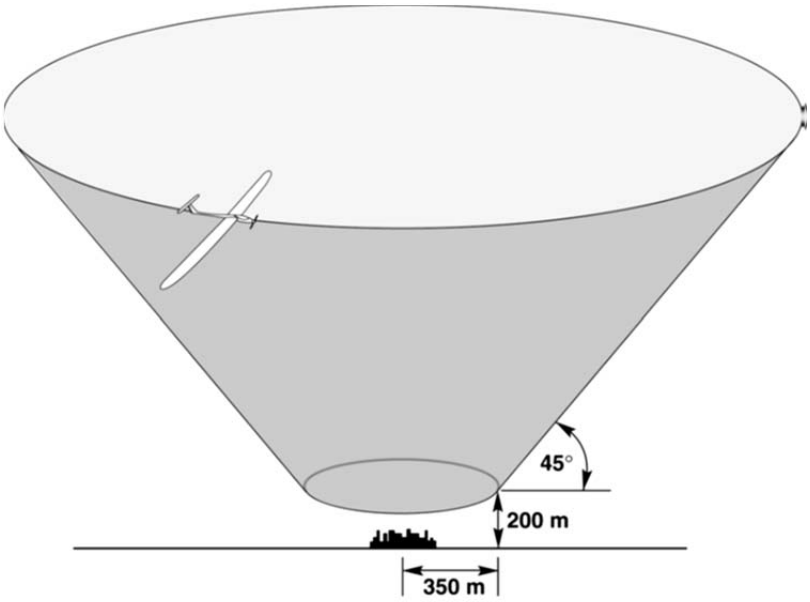

The simulations settings for the UAV were 12 m/s for the aircraft velocity and a minimum altitude floor of 200 m.

Figure 2. Mission Airspace Cone Boundary during Allen's Simulation. Source: [1].

Allen's research showed that an electric UAV with two hours of endurance could increase its endurance by 12 hours by using thermals. It also established that this benefit could be seen year round.

In another study, Nazli Kahveci and Petros Loannou looked at is about maneuvering a UAV across dense thermal regions using the minimal spanning tree algorithm that covered thermals detected in each division. They found that the physical requirements and the flight limitations could be modeled mathematically to develop algorithms that define flight paths [2].

Daniel J. Edwards developed and implemented on board an algorithm for thermal localization using the rate of change of energy and the speed polar of the glider. By applying the techniques of geo-localization, adaptive grids, and

nonlinear regression correlation, the estimation of the centroid of the thermal could be determined. Edwards concluded the flight path algorithms developed could improve the performance of the UAV in high-endurance missions without adding weight [3].

Andrew Klesh and Pierre Kabamba explored the use of solar panels embedded in the UAV wings to develop energy-optimal path planning. Their report explained that the energy collected could be used to drive the propeller, and the considerations of aircrafts kinematics and energy collected and lost were used to develop mathematical models related to the bank angle of the plane. The authors addressed the problem as an optimal control problem having as inputs, velocities and bank angle. Klesh and Kabamba found the use of the power ratio (collected energy over energy loss) for the prediction of the optimal path and for the fulfillment of the requirements of loitering perpetually in a given flight location. Their study established that "Perpetual solar-powered flight is achievable if and only if the power ratio is greater or equal to the reciprocal of the daylight duty cycle" [4].

1. NPS Students' Progress

Both professors and students were involved in the TaLEUAS project (Professors Kevin D. Jones, Vladimir Dobrokhodov, and Isaac Kaminer, thesis advisor, co-advisor, and second reader, respectively).

Klas Andersson, a Ph.D. student, and others developed an algorithm with the objective of finding thermals using cooperative teams of UAVs [5]. This report explained how the probability of finding a thermal increases significantly by using 2 or more UAVs working together. The algorithm developed was simulated by the author taking the work developed by Allen in [1] as a foundation with the extension of two flying bodies. This first investigation led Andersson et al. to conclude that many low-performance, cooperative UAVs increased the probability of detecting thermals over a fewer high-performance UAVs (Figure 3).

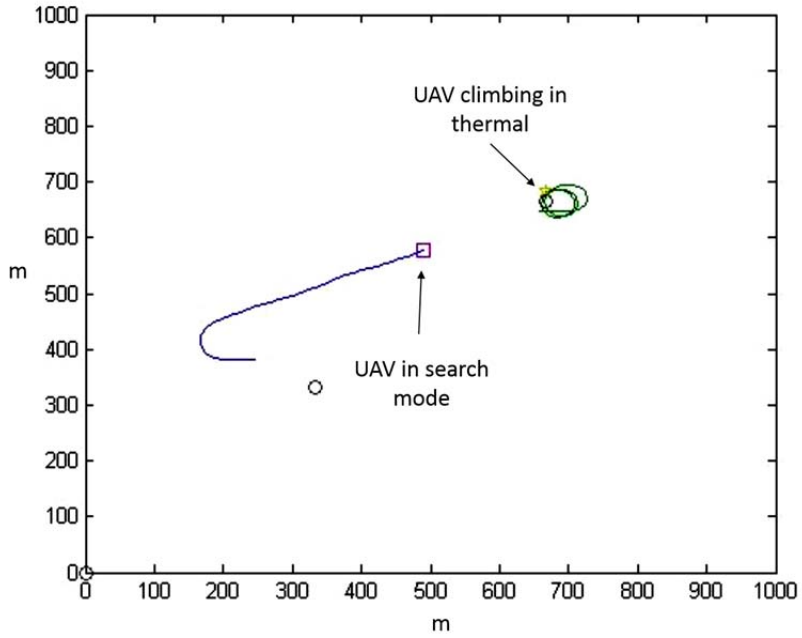

Figure 3. Simulation of Cooperating UAVs. Source: [5].

Andersson's et al. contribution was to include a theoretical analysis of stability and convergence of the algorithm developed in [5]. The analysis was developed by using an exponential Gaussian function to characterize the updraft field in a thermal proving the asymptotical stability of the controller at the equilibrium state given [6].

Andersson et al. also studied the stability and effectiveness of the thermal controller developed is shown in Figure 4, with notable wind shear at about 600 meters of elevation, changing the track of the thermal. The algorithm was evaluated during flight tests using the SBXC airframe with results that verify the theoretical stability obtained in their previous work [7].

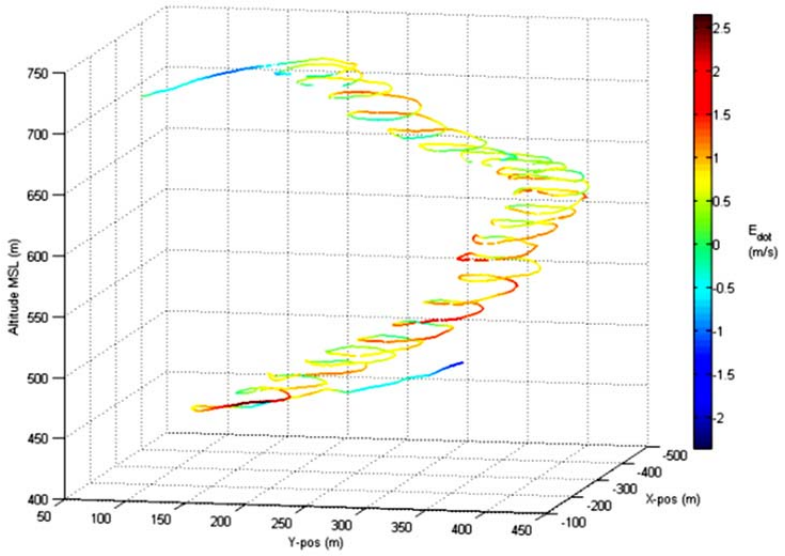

Figure 4. Tracking of Thermal during Climb. Source: [7].

Nahum Camacho, a graduate student at NPS, studied the use of multiple UAVs able to harvest energy from using photo-voltaic energy, and thermals detection (Figure 5).

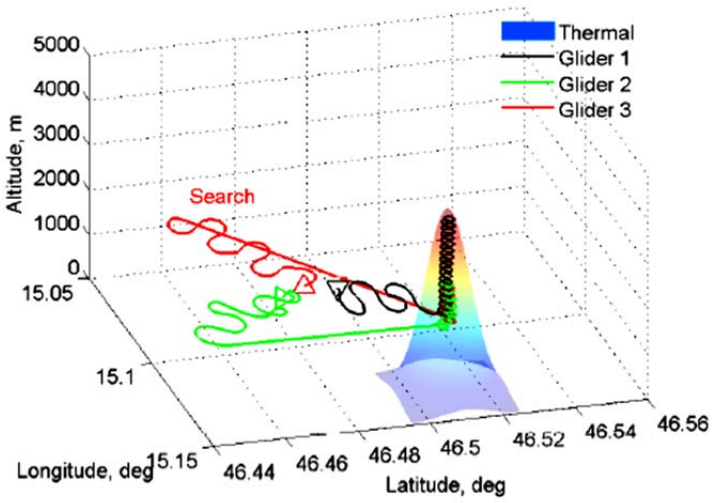

It can be seen how glider 1 detects the thermal and shares the information with numbers two and three.

Figure 5. Cooperative Flight of Three Gliders. Source: [8].

His research explored the technologies required to take advantage of this energy for mission planning and execution scenarios. Key among these technologies were photo-voltaic solar panels, batteries, the power management system, glider properties, convective thermal detection, and collaborative environment sensing by utilizing a recursive Bayesian estimation [8].

Camacho's thesis detailed how the Condor flight simulator software was used to test the implementation of the algorithm developed to get the results previously mentioned [9].

Robert Fauci, an NPS graduate student, modified an electronic circuit that optimizes the solar energy absorption, the maximum power point tracker, such that it could act as an efficient charge controller for the lithium batteries. This contribution was capable of showing the energy demand of propulsion, avionics and payload components and also allowed for tracking the energy storage and flux of energy by the batteries during the operation of the UAV [10].

C. THESIS OBJECTIVES

The core focus of this thesis is to develop a methodology intended to produce an aerodynamic model to simulate the air flow around the SBXC airframe, having as the ultimate goal to try to reproduce the same performance of the UAV in real flight for nominal angles of attack and gliding velocity developed by John Ellias [11] and Dan Edwards [12] .

As a secondary goal, this thesis provides students of aerodynamics with a CFD simulation process set up with the goals of:

- Have a meshing quality good enough to validate the results.
- Detail the process required to derive data from the main simulation results.

D. FORMULATION OF THE PROBLEM

Based on these objectives, there is a step-by-step procedure to generate a geometry using CAD tools such as Solidworks and then analyzing it using CFD tools such as Ansys-CFX:

- Modeling the fluid domain using cavity tools and sketch picture technique
- Choosing the right meshing technique based on the capabilities of each one
- Implementing the boundary conditions (BC)
- Selecting the appropriate solver setting
- Interpretation and validation of the result in the Ansys environment
- Deriving the aerodynamic data

The integration of the capabilities listed previously allows for the creation of a set of instructions to define an aerodynamic simulation using computational tools.

E. BACKGROUND AND PREVIOUS RESEARCH

Let us imagine the need to study a complex system. The first thing to do is to describe the system behavior with a governing mathematical expression that lays in the group of differential equations such as the Navier Stokes equations and turbulence models with boundary conditions.

Based on the complexity of the problem and the advantage of the computers, numerical analysis techniques can be applied to solve the equations.

1. FEM and CFD

The finite element method (FEM) is a technique that can be applied to problems related with complex geometry such as gliders, based in specific given conditions.

The FEM involves the partition of the problem domain into a large number of subdomains divided by nodes. Every single subdomain is called a finite element [13]. Nodes and elements can be identified clearly in Figure 6:

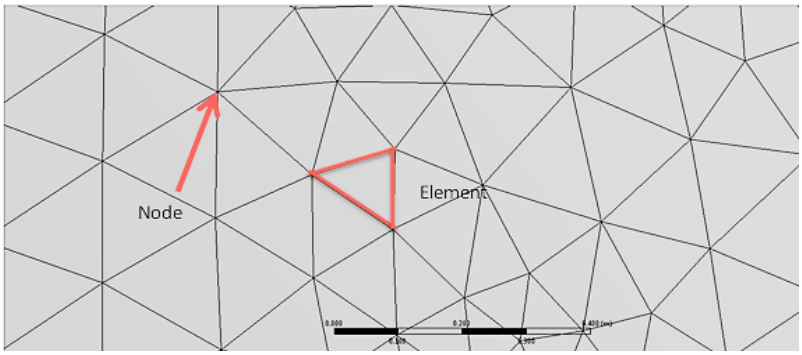

Figure 6. Identification of Nodes and Elements in a Two Dimensional Mesh.

The FEM technique can be applied to many of engineering phenomena. Currently, most commercial Computer-Aided engineering (CAE) programs are based on FEM, allowing the users to solve complex problems in different areas of engineering, like structural analysis, thermo-fluids and multibody dynamic interaction (MBD).

The area of FEM covered in this thesis is the fluid analysis, commonly known as a Computational Fluid Dynamic (CFD). The CFD programs are capable of doing Finite Element Analysis (FEA) of fluids in motion described by Navier Stokes equations as governing equations and being solved by iterative numerical analysis [14].

Following are some of the benefits of CFD:

- High level design for thermo-fluids projects with high fidelity results with the goal of reducing the time-costs process before going into production
- Evaluation of performance of complex engineering systems to aid in optimization of the product

- Capability to simulate a expensive experimental test as many times as desired

2. Performance Testing of RNR's SBXC Using GPS

John Ellias [11] developed a performance test for the SBXC airframe using a Garmin Etrex Vista Global Positioning System (GPS) with the objective to obtain the sink polar of the glider.

The Garmin GPS was collocated under the wing with a small offset from the center of gravity.

a. Testing Procedure

The GPS was programmed to record position, speed, and altitude every 0.01 miles. The test period covered approximately six weeks with four separate days of flight tests.

The launches were made with an electric winch that protruded an initial altitude of about 152 meters above ground. An important fact that the author considered was to determine the trim setting for each run to try to get a constant airspeed during the flight. As soon as the flight ended, the trimming conditions were changed to fly at a different airspeed. The range of airspeeds was from just above stall to a shallow dive.

b. Results and Conclusions

Ellias made a post-flight analysis to determine the sink rate and the lift over drag ratio for the speeds tested (Table 1).

Table 1. Ellias SBXC Performance Test. Source: [11].

SBXC FLIGHT TESTING

Flight #	Date	Trail edge camber	Ground Speed (1) mph	Wind	Best L/D	Sink rate fpm
1	6-Jan-02	neutral	29	0	26	98.2
2	12 Jan 02 - 1	neutral	21	0-3 mph	25.5	72.5
3	12 Jan 02 - 1	neutral	no speed data (2)	0-3 mph	30	N/A
4	12 Jan 02- 2	neutral	26	0-3 mph	28	81.7
5	12 Jan 02- 2	neutral	no speed data (2)	0-3 mph	19.5	N/A
6	12 Jan 02- 3	up 3 deg	no speed data (2)	0-3 mph	11	N/A
7	12 Jan 02- 3	neutral	no speed data (2)	0-3 mph	28.7	N/A
8	12 Jan 02- 3	neutral	no speed data (2)	0-3 mph	23	N/A
9	26-Jan-02	neutral	21.6	3-5 mph	25.5	74.5
10	26-Jan-02	down 5 deg.	20.5	2-4 mph	29	62.2
11	26-Jan-02	neutral	25.5	1- 3 mph	21	106.0
12	26-Jan-02	neutral	33.3	1- 3 mph	19.5	150.3
13	18-Feb-02	nuetral	38	0-1mph	15	222.9
14	18-Feb-02	neutral	55	0-1mph	9	537.8
15	18-Feb-02	down 5 deg.	24.5	0-1mph	30	71.9
16	18-Feb-02	neutral	25	0-1mph	24.5	89.8

(1) Ground speed based on equal upwind and downwind legs
(2) Speed data was lost during download from GPS to PC

In his report, Ellias showed a sink-rate plot for all the speeds of the glider (Figure 7); he also mentioned the second order polynomial curve fit that he selected to describe the sink rate of the plane. He concluded that by knowing the sink rate of the glider, an optimal velocity could be chosen for different flight conditions.

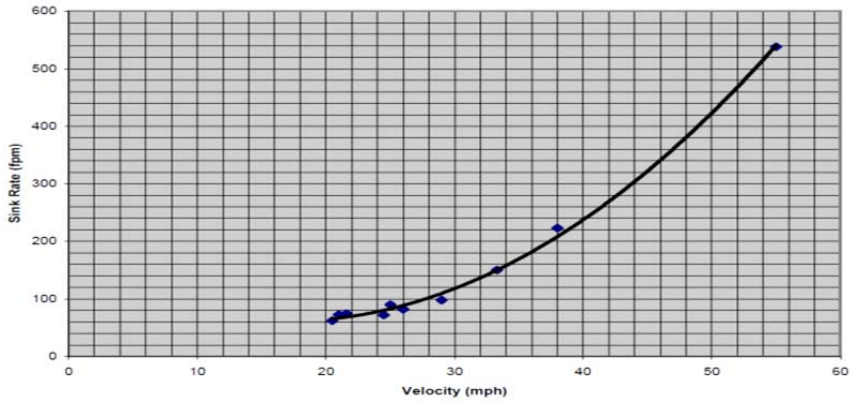

The velocity in the x axis refers to ground speed.

Figure 7. Ellias Sink Rate Plot. Source: [11].

3. Performance Testing of RNR's SBXC Using Piccolo-Autopilot

Dan Edwards ran a performance test of the glider by using an autopilot with the goal to update and compare the data obtained by Ellias. Edwards's intention was to generate the sink polar of the glider, finding the minimum sink speed, finding the speed for maximum L/D, and creating a speed to fly curve [12].

Edwards used the Piccollo Plus autopilot from Cloud Cap Technologies to collect flight data. The autopilot was installed just forward of the wing. The autopilot characteristics are mentioned in the report and are as follows [12]:

- 4hz GPS unit
- Air data system and inertial measurement unit
- Hardware capable to perform airspeed hold maneuvers and re-set for new air speeds and waypoints
- The communication link is via a 900 MHz serial link

a. Testing Procedure

The author stated that the Piccolo was configured to record flight data at 20 Hz, and the test procedure follows:

- The glider was launched with a winch to an initial altitude of 182 m.
- Activation of the autopilot.
- The flight path commanded to Piccolo was straight and with a constant airspeed.
- Data was downloaded through the Piccolo Operator Interface (Piccolo software) after a day of testing.

b. Results and Conclusions

Edwards commented that the sink rate and airspeed were averages of a minimum of 10 seconds of data during the steady-state flight of the glider (Table 2). Based on the results, he proposed a sink polar Equation (1.1) and compared this to the sink polar plot of Ellias data:

$$Vert = -0.0095V^2_{horiz} + 0.3782V_{horiz} - 4.6072 \quad (1.1)$$

Table 2. Raw Data and Computed Parameters from Flight Testing. Source: [12].

	Run #	Air Speed (kt)	Sink Rate (ft/s)	Horiz Speed (kt), 11 lb scaled	Sink Rate (ft/s), 11 lb scaled	L/D
Elias (11 lb)	1	25.2	-1.64	-	-	26.0
	2	18.2	-1.21	-	-	25.5
	3	22.6	-1.36	-	-	28.0
	4	18.8	-1.24	-	-	25.5
	5	22.2	-1.77	-	-	21.2
	6	28.9	-2.51	-	-	19.5
	7	33.0	-3.72	-	-	15.0
	8	21.7	-1.50	-	-	24.5
Edwards (11.15 lb)	9	24.0	-2.11	23.7	-2.1	19.2
	10	31.0	-2.53	30.6	-2.5	20.7
	11	20.5	-1.69	20.2	-1.7	20.5
	12	18.0	-1.43	17.8	-1.4	21.2
	13	24.5	-2.36	24.2	-2.3	17.5
	14	26.5	-2.45	26.2	-2.4	18.3
	15	28.3	-2.70	28.0	-2.7	17.7
	16	24.5	-2.03	24.2	-2.0	20.4
	17	24.8	-2.03	24.4	-2.0	20.6
	18	28.0	-1.94	27.6	-1.9	24.4
	19	30.0	-3.38	29.7	-3.3	15.0
	20	44.3	-10.63	44.1	-10.5	7.1
	21	39.8	-8.61	39.5	-8.5	7.9
	22	35.0	-5.91	34.7	-5.8	10.0
	23	30.0	-2.11	29.6	-2.1	24.0
	24	23.8	-1.86	23.5	-1.8	21.6

At the end, Edwards concluded that the flight data collected matched with the data obtained by Ellias, with minor differences (Figure 8).

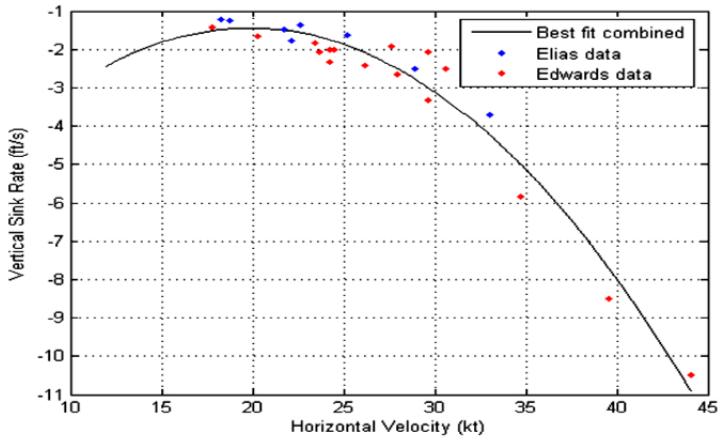

Figure 8. SBXC Sink Polar. Source: [12].

4. CFD UAV Analysis Background

CFD analysis has been a useful tool for aerodynamic studies, especially for performance evaluation and optimization of an existing model or a brand new design based on the advantages of simulating flight tests for different ranges of velocities.

Spyridon G. Kotogiannis and John A. Ekaterinaris designed, evaluated, and optimized a small UAV capable of doing reconnaissance missions. They used CATIA and CFD software to make the aerodynamic analysis with a primary goal to get maximum aerodynamic efficiency and the optimal L/D ratio to minimize the power consumption on board. Their final results in CFD matched the aerodynamic analytical results for this vehicle, and they had the capability to evaluate different winglets configuration (Figure 9) and determine the final configuration for the wing for the analyzed UAV [15].

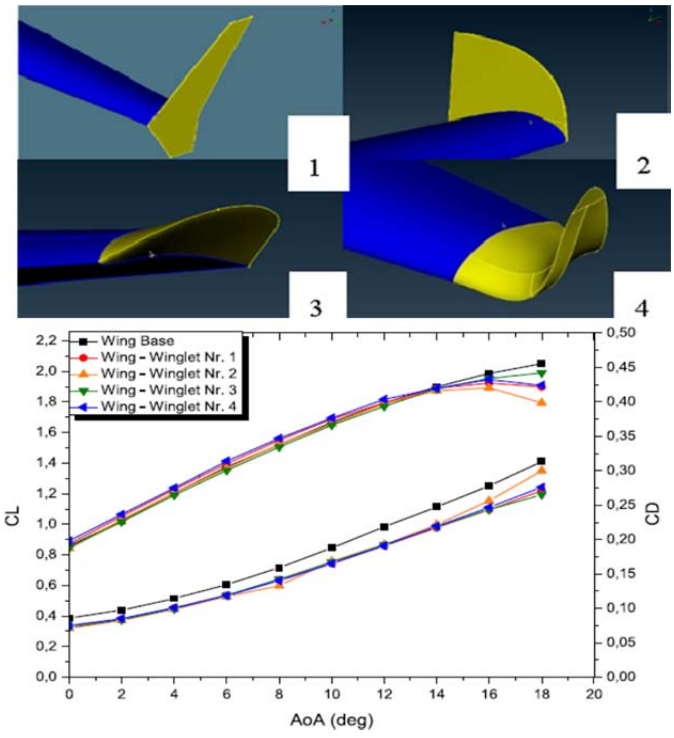

Figure 9. Comparison of Wing with various Winglets. Source: [15].

Wonjin Jin and Young Lee provided an example of the use of CFD analysis in their evaluation of the EAV-2 UAV designed by the Korean Aerospace Research Institute. The computational methodology that the authors followed started with the analysis of low Reynolds number regime airfoils using XFOIL software; next, ANSYS-FLUENT was used to simulate the aerodynamic performance of the UAV, ending with a mesh of 20 million of cells, 12 inflation layers, a non-dimensional wall distance with Yplus values < 5, and the first cell from the surface programmed to be $2x10^{-4}$ meters [16]. These concepts are described in Chapters III and IV. The results of the computational analysis using the *Spalart-Allmaras* turbulent model allowed the designers to select a more efficient airfoil for the optimized model, and they also were able to reduce the total drag by 43%, and by 14% compared with a previous model EAV-1B [16].

Panagiotou, Salpingidou, Kaparos, and Yakinthos developed a study about a medium-altitude long-endurance unmanned aerial vehicle (MALE UAV). The report included a CAD-CFD design phase and a verification phase using a three dimensional (3D) printed scale model of the designed glider inside a wind tunnel [17]. The CFD software used by this team was ANSYS-CFX with a mesh created with 20 inflation layers to capture the boundary layer regime. Their report covered the airframe design involving aerodynamic analysis of the parts of the glider and also indicated the method used to design the control surfaces of the plane.

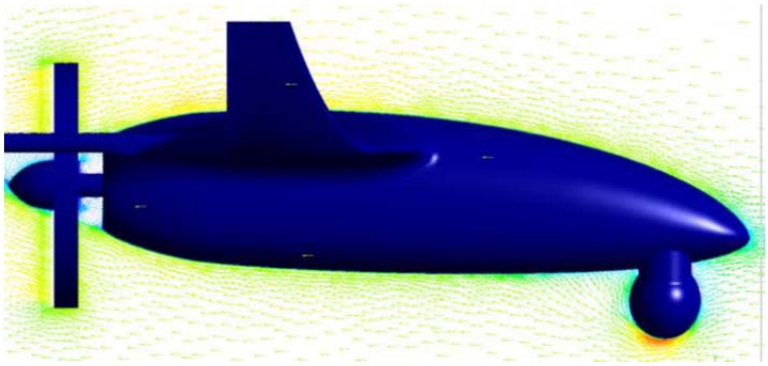

Figure 10. Flow Development around the Fuselage. Source: [17].

F. THESIS OUTLINE

The next part of this thesis focuses on the development of the analysis procedure and the post simulation analysis of the results for the aerodynamic data. The structure of this thesis is progressive, with each chapter serving as a step to follow in the simulation process.

In Chapter II the modeling of the SBXC airframe and the fluid environment that the glider is immersed in are explored. First, details of the model construction in Solidworks are provided, using pictures and scale functions. Next, details about the sizing procedure for the fluid domain and the importation method from Solidworks to ANSYS CFX are given.

Once the fluid domain is in CFX, the meshing process is the next step. Chapter III is devoted to understanding the different meshing techniques, how to evaluate the mesh quality, and how to properly model the boundary layer phenomena. The implementation of the Boundary Conditions (BC) are also given along with the computational solver setting suitable for the NPS Hamming cluster for large computational jobs.

Issues related to post-processing, or the analysis of the simulation are given in Chapter IV. For aerodynamic analyses in CFD, three important characteristics have to be studied carefully: non-dimensional wall distance (Yplus value), pressure contours on the body, and velocity profiles on the wing that show boundary layer behavior over the wing. The different techniques to make this analysis, including the derived data from the simulation results are discussed in this chapter.

Comparisons with real flight data obtained by [11] and [12] are detailed in Chapter V. The conclusion shown in Chapter VI will focus on how the results of the research can be used to validate the feasibility of the computational method chosen and the process developed.

The Appendix contains an instruction sheet that details the procedures used here to set up simulation using Solidworks, ANSYS CFX and Hamming, and might be thought of as a gouge-sheet for those that wish to perform similar studies.

II. MODELING THE GLIDER AND THE FLUID DOMAIN

This chapter will outline the procedure used to create the SBXC glider computer model from the real airframe and the considerations that need to be taken in order to determine the correct sizing for the fluid domain. It concludes with the last step of the modeling method which brings the fluid domain and the airframe together in the same volume.

A. INTRODUCTION TO SBXC GLIDER DESIGN

The SBXC glider was designed using the S2048 airfoil as a base. This airfoil was developed as a redesigned HQ2/9/RGB airfoil with the main characteristic of more gradual pressure gradients in the lower and upper surfaces to maintain laminar flow [18]. Figure 11 shows the airfoil geometry and the behavior of the airfoil at different Reynold Numbers using the lift and drag coefficient obtained experimentally.

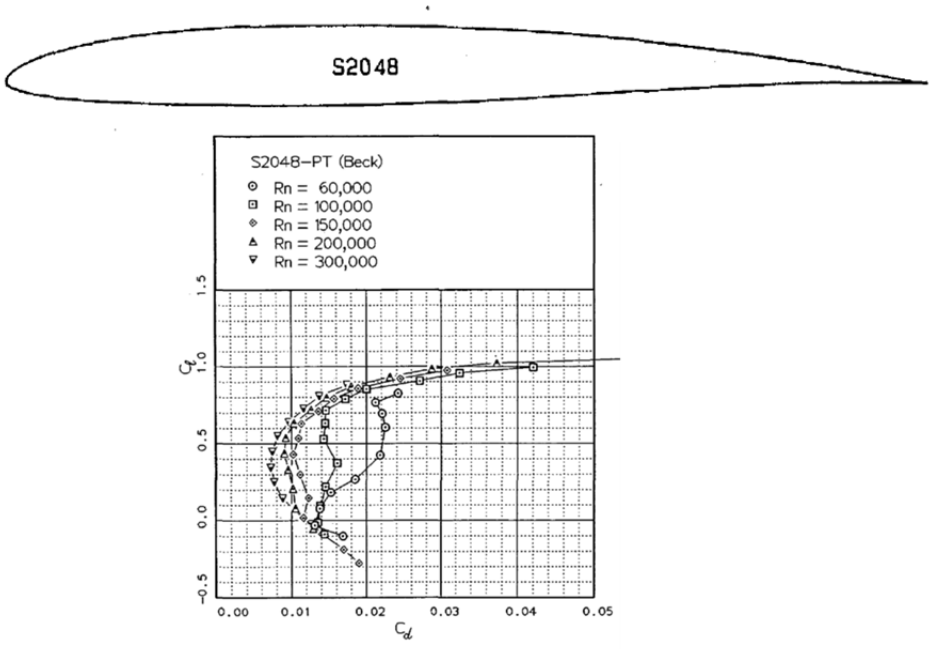

Figure 11. S2048 Airfoil Behavior in Different Reynolds Numbers. Source: [18]

However, during the manufacturing of the molds for the SBXC glider, the thickness of the S2048 airfoil was increased by about 7.4%; therefore, the necessity to evaluate the performance of the wing to verify that the machining process did not destroy the laminar flow qualities of the original airfoil.

B. MODELING GENERATION

The modeling of the glider and the fluid domain was done in Solidworks. Two techniques were used to solve the task. The first one was called picture sketch and was used to model the fuselage. The second one was for the wing model and it was based on a computer program developed by Professor Kevin D. Jones capable of creating numerical coordinates that describe the airfoil profiles at different positions along the wing span, based on an airfoil database from UIUC.

1. Sketch Picture and Airfoil Coordinates Generator Software

The technique used to generate the geometry for the fuselage and horizontal stabilizer data from the real SBXC was the “Sketch Picture” technique. This method is based on using a picture of the plane as a drawing base for the sketch that will be manipulated to match the real scale of the airframe (Figure 12).

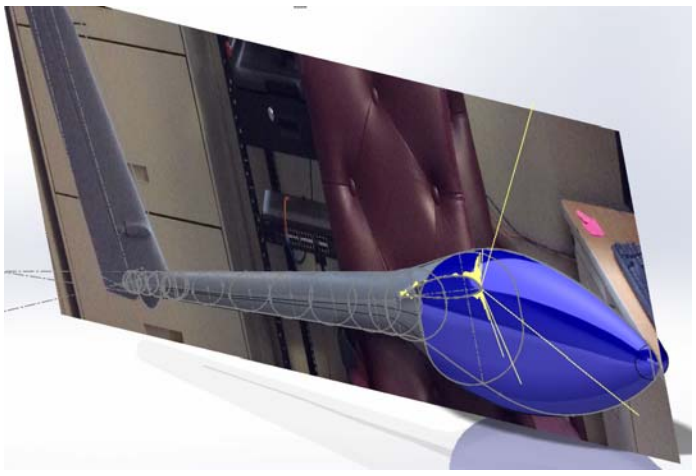

Figure 12. Picture Sketch Technique Applied to the SBXC Fuselage.

The first step to enable this option in Solidworks was to select the plane to insert the picture into, and the second step was to activate the option under the sketch tools menu located in the tools bar. When the picture was placed the scale had to be modified to match the real dimension of the body to create the first two dimensional sketch, and the same procedure was made in the perpendicular plane to create the other part of the sketch. Finally, a loft operation was used to connect two sketches and create the solid volume of the body.

The airfoil coordinate generator program was used to sketch the wings, by creating a number of airfoils sections from the root of the wing to the tip that could be connected with lofts in Solidworks. The input data for each profile is shown in Table 3. The output data for each section was a TXT file which contained the coordinates of the points that needed to be sketched. The code used to generate this data was developed by Professor Kevin Jones.

Table 3. Airfoil Coordinates Generator Inputs Data.

# profile	# points desired	Thickness scale	Cord length	X offset	Y offset	Z offset	File name
1	201	1.074	300	0	0	0	Section1.txt
2	201	1.074	226	74	42	1252.5	Section2.txt
3	201	1.074	217.75	80.92	50.44	1352.5	Section3.txt
4	201	1.074	209.25	88.08	58.88	1452.5	Section4.txt
5	201	1.074	200.75	95.25	67.32	1552.5	Section5.txt
6	201	1.074	192	102.67	75.76	1652.5	Section6.txt
7	201	1.074	183	110.33	84.20	1752.5	Section7.txt
8	201	1.074	172.50	119.50	92.64	1852.5	Section8.txt
9	201	1.074	156	134.67	101.08	1952.5	Section9.txt
10	201	1.074	142.19	147.67	105.3	2002.5	Section10.txt
11	201	1.074	120.50	168.83	109.52	2052.5	Section11.txt
12	201	1.074	104.77	184.23	111.63	2077.5	Section12.txt
13	201	1.074	84	204.67	113.74	2102.5	Section13.txt
14	201	1.074	70.81	217.69	114.79	2115	Section14.txt
15	201	1.074	54.68	233.65	115.85	2127.5	Section15.txt
16	201	1.074	33.58	254.59	116.90	2140	Section16.txt
17	201	1.074	19.51	268.58	117.43	2146.2	Section17.txt
18	201	1.074	1	287.00	117.96	2152.5	Section18.txt

The thickness scale is a factor that multiplies the normal thickness of the root airfoil.

The importation process of the coordinates values (*.txt files) to Solidworks can be found in [19].

To create the volume shape for the fuselage and the wings (Figures 12 and 13) a loft feature was required. This command is mandatory as it will allow the creation of curve volumes in full solid without empty spaces.

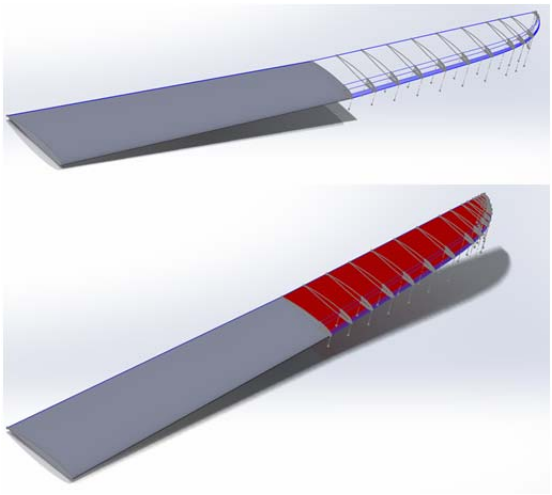

Figure 13. Left Wing of the SBXC Glider created with Professor Jones's Software.

2. Generation of Fluid Domain

As mentioned, the fluid domain is the space where the fluid surrounding the body is simulated. There is no fixed rule to determine the size of the boundary box but, from experience, the size has to be approximately ten times bigger than the root chord length of the wing in all directions. The modeling of the fluid domain can be considered as the test volume and should be large enough such that the BCs do not produce non-physical features in the flow.

An almost cubic shape for the domain was used; therefore, based on the dimensions of the SBXC (Table 4), the first attempt was 7x7x4 meters, but after the post-analysis, the boundary box was reduced to the final dimension of 6.52x4x4 meters.

Table 4. SBXC Dimensions.

Wing span	4.28 meters
Wing area	0.96 square meters
Fuselage length	1.94 meters

The dimensions in this table were obtained using Solidworks and the NPS SBXC glider. The dimensions mismatch with the SBXC manual by 0.03 meters in the wing span and 0.03 square meters in the wing area. It has to be mentioned that all the gliders mismatch the manual values due to the construction process.

To create the fluid domain as a volume with the glider model subtracted, an assembly was required. Based on the geometric symmetry of the glider, the assumption of symmetry was made; therefore, only half of the domain was required.

The glider model was placed in the X-Y plane created by the face with a dimension of 6.52x4 meters and by making coincidence the midpoint of the fuselage with the midpoint of the face (Figure 14).

Figure 14. Assembly of the SBXC Glider with the Fluid Domain.

Finally, the subtraction of the SBXC body had to be done to produce the fluid space. For this step, the cavity tool was used to remove the volume of the glider model from the fluid domain (Figure 15). It has to be mentioned that the

cavity tool did not accept bodies built from surfaces, rather than volumes; therefore, using the loft command during the modeling of the glider was required.

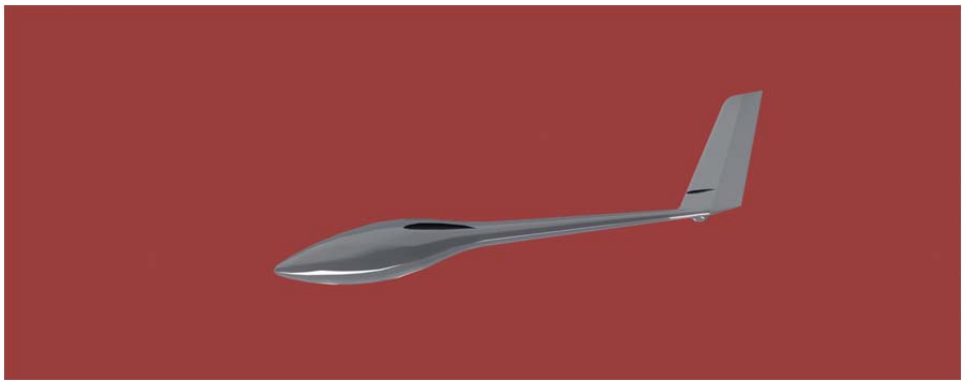

In the figure, the correct implementation of the cavity tool can be seen.

Figure 15. Final State of the Fluid Domain.

3. Import the Fluid Domain into ANSYS CFX

The goal of this step was to share the fluid domain that is desired to analyze with the computational software selected for use; therefore, the importation of the CAD model into the CFD software was a key point in the CFD process. ANSYS CFX allowed Parasolid files to be used as geometry models. The transfer process between Solidworks and CFX was the following:

1. Save the fluid domain as a parasolid file (extension: *.x_t).
2. Open ANSYS Workbench.
3. Drag Fluid Flow (CFX) from ANSYS tool box into ANSYS project schematic area.
4. When the CFX block is loaded, right-click on geometry and browse the fluid domain file.
5. A green check mark will appear when the process is finished.

III. PRE-PROCESSING

Pre-processing involves setting all of the information required to be evaluated into the computer analysis program. The analyst must tell the computer the conditions of the work and how he or she wants it to be solved. Setting the instructions is a critical step because if the conditions of the problem are not well defined, this will impact the quality, trustworthiness, and relevance of the results.

A. OVERVIEW

A closer look at the process of meshing is made in this chapter. Recall that meshing is the transition from the entire fluid domain to the small division of finite elements. This chapter also explores how the BCs of the aircraft surface are defined in the fluid domain and discusses the final step of pre-processing, which involves letting the software know how to process the information given by the mesh and the BCs.

The NPS supercomputer Hamming was an important tool used during the development of this project. This section covers a brief introduction to the cluster and the correct way to submit large CFD files to accelerate computational times without running out of computational resources.

B. MESHING

A mesh can be defined as the group of finite elements that form a domain to be analyzed with computational methods. ANSYS CFX has different options and techniques that help the analyst to develop a mesh easily, depending on the fluid analysis to be performed. In Figure 16, the meshing application for ANSYS can be seen:

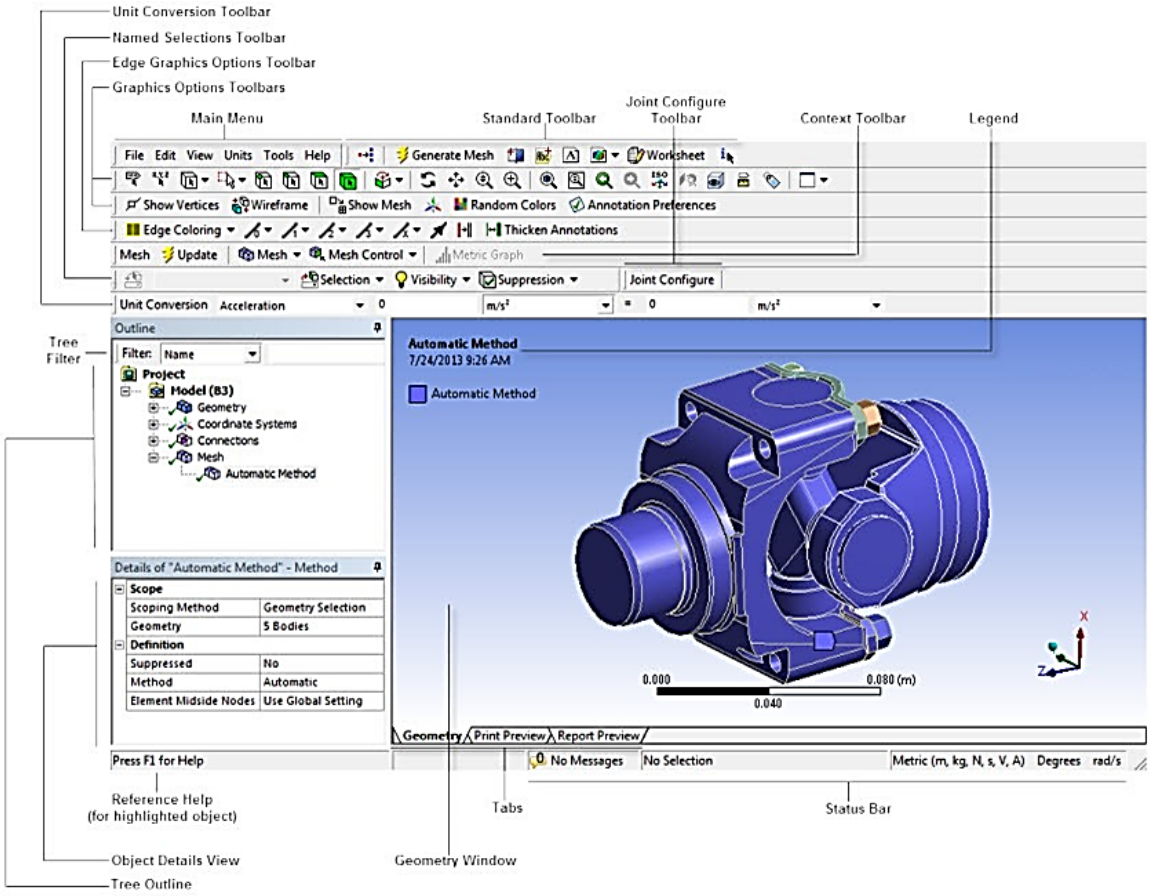

Figure 16. Meshing Application Interface. Source: [20].

The meshing process can be broken down into three phases. Phase one specifies the type of mesh based upon the domain. Phase two is to preview and generate the mesh selected. Phase three is dedicated to evaluating the quality of the mesh. Frequently this last step cannot be performed until a trial solution is computed.

1. Meshing Advance Size Function Available for Fluids Dynamics

A size function in CFD is an embedded mathematical function that describes the geometry of the finite element designated to use in a specific fluid domain. The selection of the right size function is a strong determinant in the accuracy of the results in the simulation.

ANSYS-CFX has four size function options: Fixed, Proximity, Curvature, and Proximity and curvature. The characteristics of each function are explained in Table 5 and their behavior can be seen in Figure 17:

Table 5. ANSYS Size Functions Characteristics.

Size function	Characteristics
Fixed	• Constant mesh size in the whole domain • There is no refinement in zones with curvature • The maximum face size defines the surface mesh • The maximum volume size defines the volume mesh
Proximity	• Controls the mesh resolution based on the distance between regions (large distance, big element) • High number of elements across a gap • Transition of the cell size depends of the grow rate specified by the user
Curvature	• Determines the edge and face size based on the curvature normal angle specified by the user • Finer curvature angle, finer surface mesh • Transition of cell size is defined by the grow rate specified by the user.
Proximity and Curvature	• Basically, it is the combination of the Proximity size function characteristics and Curvature size function characteristics.

This information was gathered using [20] and [21].

Based on the characteristics of the fluid domain created for the SBXC airframe and the necessity of gathering a large numbers of cells near the leading edge of the wing, the size function that fit the best was Proximity and Curvature.

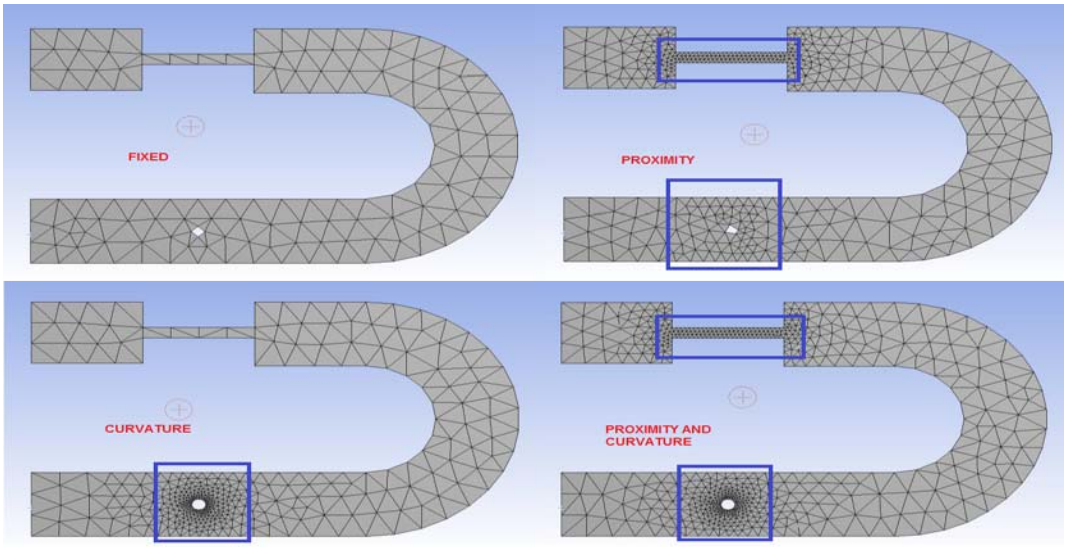

Figure 17. Size Functions Behavior. Adapted from [21].

2. Inflation Techniques for Fluids Dynamics

The objective of the inflation technique is to generate refine, orthogonal finite elements close to the walls of the body with a suitable size to model the boundary layer behavior of the fluid. The available techniques in ANSYS are described in Table 6:

Table 6. ANSYS Inflation Techniques. Adapted from [21].

Inflation Technique	Objective
Smooth Transition	The main characteristic of this technique is to create a smooth growth in the volume of the adjacent elements based on the surface mesh in the wall.
First Layer Thickness	This technique maintains the height of the first element constant in all the inflation layers created. The height is defined by the user.
Total Thickness	Maintains constant total height in all the inflation layers
First Aspect Ratio	The height of the inflation layers is defined by the aspect ratio of the inflation layers that are extruded from the first inflation layer created on the base of the surface.
Last Aspect Ratio	This technique uses the first layer height defined by the user and aspect ratio controls to define the inflation layers geometry.

The two best inflation options that both allowed for control of the first layer height were the first layer thickness (Figure 18) and last aspect ratio (Figure 19). By evaluating the element quality (Chapter III, Section III) and the Yplus value (Chapter IV, Section C) the final choice for inflation technique was the last aspect ratio with a first layer height of 1 x 10^{-5} meters due to the fact that it allowed for the best representation of the description of the boundary layer without creating severe disturbances in the element shape. The biggest inconvenience of using the first layer inflation technique is the constant value of the height creating a poorly shaped elements just outside the inflation layer.

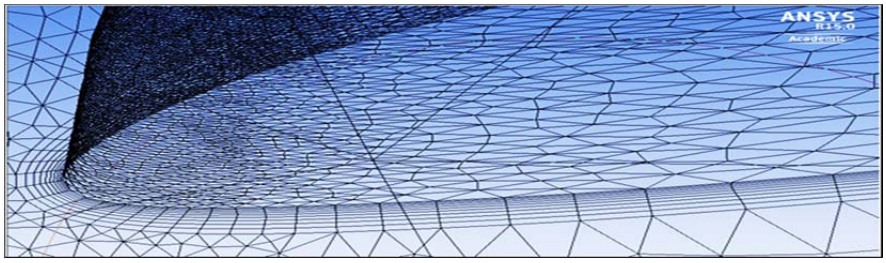

Figure 18. First Layer Inflation Applied to the SBXC Wing.

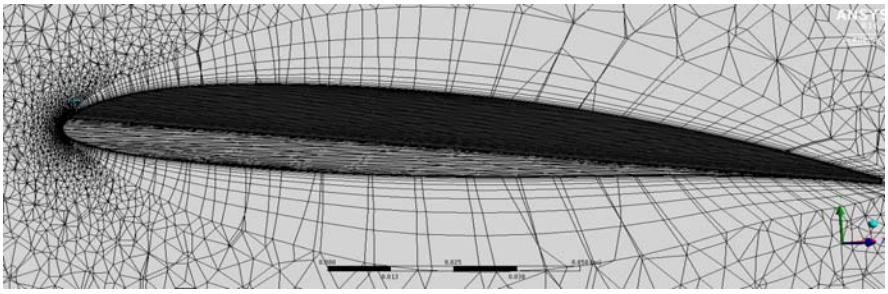

Figure 19. Last Aspect Ratio Inflation Applied to the SBXC Wing.

3. Mesh Quality

The quality of the mesh depends on many factors. Key among these factors is the element shape. Element shape can be evaluated by making a cut into the mesh using the ANSYS section tool and visually inspecting the area. The objective is to identify strange element shapes that do not belong to the element pattern. In Figure 20, a good distribution of the element shapes can be observed.

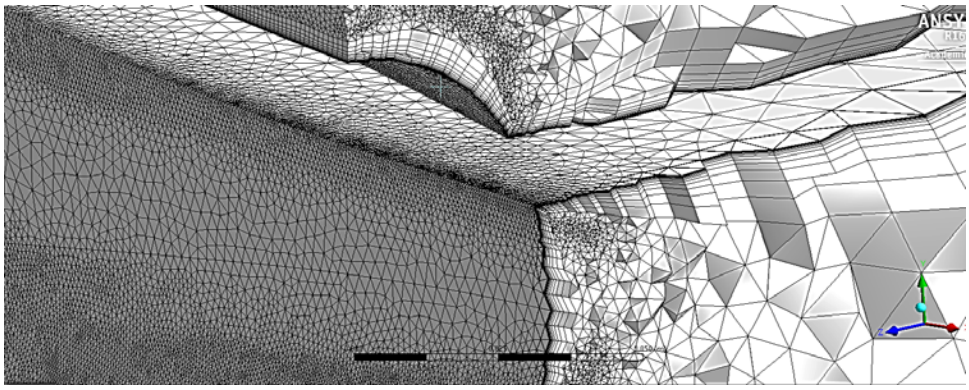

Figure 20. Section of the SBXC Fluid Domain after the Meshing Process.

Another factor to evaluate is the mesh element quality values. The mesh application in ANSYS can calculate metrics (Figure 21) of the finite elements using the total number of finite elements distributed in the fluid domain. It can be considered a good mesh if the average metric value is greater than 0.3 and if the critical regions of the fluid domain also has values of metrics greater than 0.3 (Table 7).

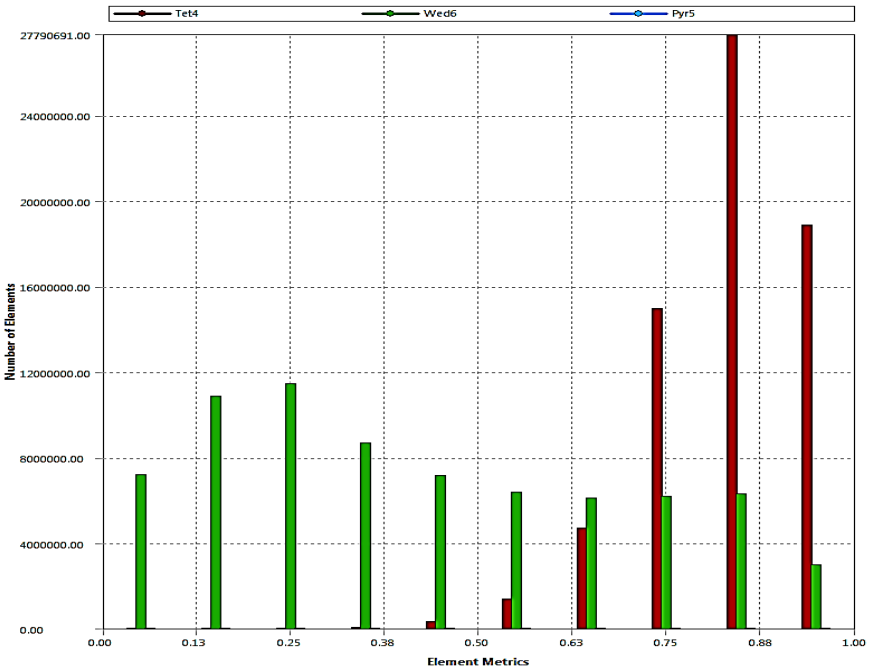

Figure 21. Element Quality Graph for the SBXC Fluid Domain.

Table 7. Element Quality Statistics Table.

Statistics	
Number of nodes	49254491
Number of elements	141111355
Mesh metric	Element quality
Min metric value	1.6312 e -004
Max Metric value	0.99998
Average metric value	0.62371

C. BOUNDARY CONDITIONS

The boundary conditions are required on all the fluid domain. The conditions need to be satisfied in order to solve the mathematical expressions that describe the physics inside the fluid domain.

ANSYS CFX allows the user to specify the type fluid to work with, temperature, type of analysis, and accuracy of the solution. All the input data mentioned can be introduced or modified in the setup division of the CFX block in the project schematic area. The setup application is also named CFX-Pre.

1. Default Domain

The default domain is the section of the CFX-Pre where the user can define all the characteristics of the fluid, the model's characteristics, and the type of analysis desired. For the SBXC glider the settings up were defined as shown in Table 8:

Table 8. Default Domain Configuration for SBXC Airframe Analysis.

Basic settings	Fluid settings
Material= Air at 25 C	Heat transfer= isothermal
Morphology= continuous flow	Fluid temperature= 25 C
Reference pressure= 1Atmosphere	Turbulence model= shear stress transport
Buoyancy model= non buoyant	Wall function= automatic
Domain motion= stationary	Transition Model= Gamma Tetha model
Mesh deformation= none	Combustion and thermal radiation= none

2. Inlet, Outlet, Wall, Opening

Based on the fluid domain geometry and the flow of the air, the BC can be specified in each face of the boundary box. CFX-Pre allows the user to select the type of BC based on the desired movement of the fluid. The options are: inlet, outlet, wall, symmetry and opening.

The inlet BC specifies the flow regime and the characteristics of mass flow in different options, including: Cartesian coordinates, cylindrical coordinates, mass flow, and normal speed or pressure. The outlet BC describes the exit of the flow using the same options as the inlet.

The opening BC is used when there is the possibility of flow entering and/ or leaving the domain. A pressure or a velocity is required to be defined. The options to define velocity or pressure values are: static and entrainment for pressure; and Cartesian and cylindrical coordinates for velocity.

A symmetry BC is used when a body to be analyzed has a symmetry plane and the applied conditions are symmetric. This BC allows considering analyzing only half of the body and to use the values calculated on the other half as they are both equal. A restriction of the symmetry condition is that the flow field also must be symmetric.

A wall condition is applied on several surfaces. The first wall condition option available for this BC is the no-slip wall and is used for viscous flow to obey the no-slip condition (total velocity is wall velocity); the second one is the free-slip wall with the goal to allow the fluid to behave with liberty but with normal velocity set to zero (flow tangency).

The BCs used for the SBXC analysis can be observed in Figure 22. The free stream velocity for the first analysis was 12 m/s; the angle of attack (AoA) was 3 degrees. It has to be mentioned that the angle construction angle of the SBXC was 7 degrees; therefore, the numeric AoA or CFX angle (CFXA) used was -4 degrees to achieve an angle of attack relative to the chord line of 3 degrees.

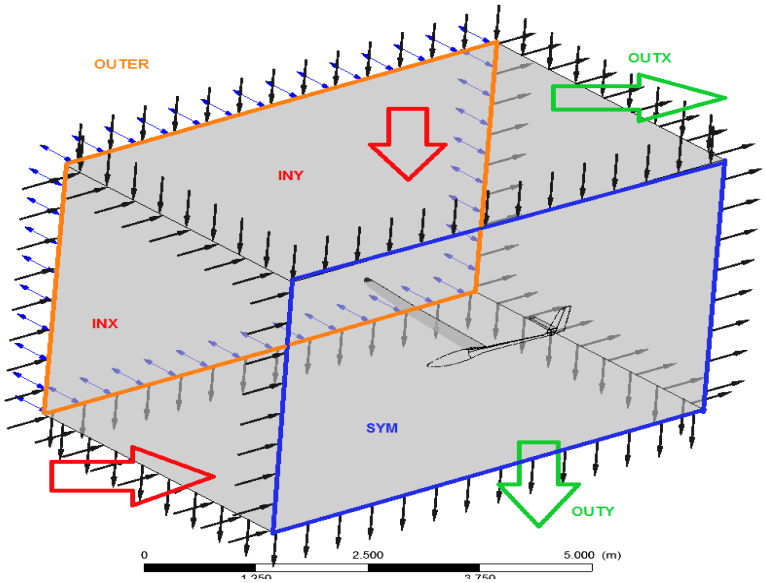

Figure 22. Boundaries Conditions for the SBXC Fluid Domain.

D. SOLVER CONTROL

The solver control option in CFX-Pre is the place to set up the desired characteristics for your solution, including: level of resolution, convergence control, and convergence criteria. Also, the solver controls show the user the types of equations that are going to be solved.

There are two ways to configure the solver control: first, the classic double clicking method involves double clicking on solver control under the outline heading and manually introducing the values, as seen in Table 9:

Table 9. Solver Control Configuration for the SBXC Analysis.

Basic settings	**Equation classes**
Advection scheme: High resolution	Continuity
Turbulence numeric: High resolution	Momentum
Max. Iterations: 150	Turbulence eddy frequency
Time scale factor: 1	Turbulence kinetic energy
Residual type: RMS	
Residual target: 0.00001	

In the equation classes setting, each equation can be configured independently. The configuration shown in this table allows having high resolution in all the equations.

Second, you can configure the solver control by using the command editor. The command editor can be opened with a right click in the solver control under outline and introducing the configuration as seen in Figure 23:

```
FLOW: Flow Analysis 1
  &replace SOLVER CONTROL:
    Turbulence Numerics = High Resolution
    ADVECTION SCHEME:
      Option = High Resolution
    END
    CONVERGENCE CONTROL:
      Length Scale Option = Conservative
      Maximum Number of Iterations = 150
      Minimum Number of Iterations = 1
      Timescale Control = Auto Timescale
      Timescale Factor = 1.0
    END
    CONVERGENCE CRITERIA:
      Residual Target = 0.00001
      Residual Type = RMS
    END
    DYNAMIC MODEL CONTROL:
      Global Dynamic Model Control = On
    END
  END
END
```

Figure 23. Solver Control–Command Editor.

E. HAMMING

Hamming is a high performance parallel computing cluster at NPS that allows the use of specialized software to solve very large solutions that require more memory and time than would be possible or practical on a workstation [22]. One of the important characteristics of Hamming is that the user can submit the desired data to the cluster from his or her own computer, allowing the user to keep working without spending his or her computational resources.

The principal advantage that Hamming offers for CFD analysis is the capability to solve meshes higher than 50 million nodes with high resolution requested in the solver in a reasonably short amount of time. The benefit of doing CFD analysis on the supercomputer is clearly seen if the comparison of complexity versus time has to be considered.

1. Hamming Configuration

Hamming's web page [22] described the supercomputer as a device that is like 800 laptops working together, providing about 3200 cores. Hamming's capabilities can be divided into three subsystems:

- Message passing interface: It is a program used for the correct communication between numerous processes during parallel computing.
- Graphic processing unit: It provides the visualization of the analyzed data.
- Grace: It is a computer configuration that allows distributing and sharing large data sets across the supercomputer nodes.

Hamming's physical characteristics are [23]:

- 59 active compute nodes
- 2962 total compute central processing units
- 12 Terabytes for total compute memory
- 270 Terabytes (plus 54 Terabytes parity) for total raw pooled storage
- 163 Terabytes for total raw local storage
- 55 Graphical processing units

2. Hamming-ANSYS CFX Communication Link

To do CFD analysis using hamming capabilities, a communication link has to be established. For this thesis, the communication software between the NPS computer lab and Hamming was MobaXterm_Personal_8.5. The software has a traditional command line environment; therefore, a group of basic commands need to be known to interact with the cluster (Table 10).

Table 10. Hamming Basic Commands.

qsub -I -X	Logs the user to a onto a compute node
qsub (file name)	Submit a file to the cluster
Module load app/ANSYS	Activate ANSYS license
cfx5pre	To call the CFX-Pre graphic window
Cfx5solve	To call the CFX5-solver graphic window
Mkdir (name)	Create a subdirectory with the selected name
ls	List the files under the subdirectory
cd (name)	Change to the named directory
qdel	to delate a running project

The commands shown in the table were the ones most frequently used during the development of the project, but more commands can be found in [22].

To submit an ANSYS CFX job to Hamming, two things are necessary. First, one must create a script with all of the commands that establish the Hamming-ANSYS link. Second, one must create a file that contains the mesh, setup, and solver control information for the simulation. This file is better known as a definition file (*.def).

To create a definition file, the first thing to do is locate the file with CFX extension (*.cfx) under the folder created by ANSYS during the meshing and setting up process. Next, copy the CFX file and open it in Hamming by using the command list in the order shown in Figure 24:

cd “your_folder”	Change from home directory to the subdirectory created by the user.
ls	Shows the list of files located in the subdirectory.
qsub –I –X	Enables a node for the interactive session with hamming using the graphic interface.
module load app/ansys	Enables Ansys to be used.
cfx5pre	Call the CFX-Pre application

Figure 24. Command List to open CFX-Pre in Hamming.

When the CFX-Pre application is open, browse for the file (*.cfx) and wait until the loading process is complete. Finally, select the option called *write a solver input file* located in the solution bar, as seen in Figure 25:

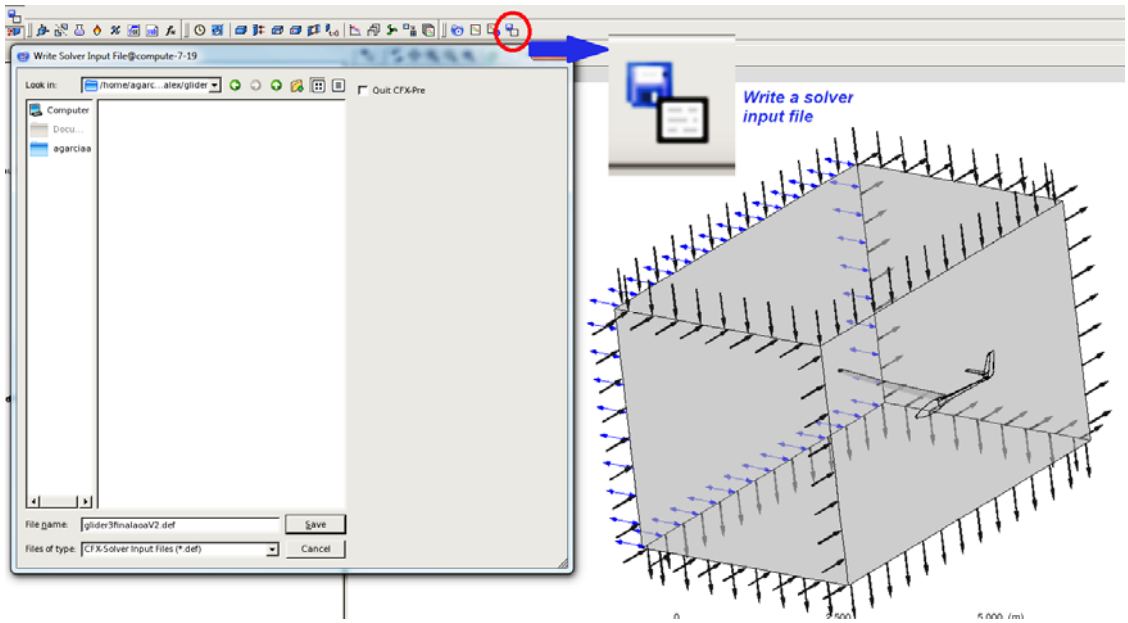

Figure 25. Creation of a Definition File in Hamming Environment.

The characteristics of Hamming have to be considered for the creation of the submission script. The cluster allows using multiple nodes with multiple processors on each node, but it is highly recommended that the user use only one node with multiple cores to increase the efficiency of the computational resources due to the size of the simulation file. In Appendix, the distribution and meaning of each command can be observed. The file can be created in any text editor that allows to save as **.sh* file.

An important reminder is to double check the numbers of nodes the mesh created. If the mesh has more than 20 million nodes, like this project configuration, a large partition method is required (Appendix-Hamming Communication Script), but if the mesh contains less than 20 million of nodes, the “part” commands can be omitted.

The final step is to submit the job using the script created. The steps for this process are the following:

- Be sure that the definition file and the script are saved in the same subdirectory in Hamming.
- In the Hamming command window, type “qsub *name of the script.sh.”*
- Hamming will give a job number, and the user can track the status of the simulation using “qstat.”
- Finally, the user can visualize the convergence ratio, using the graphic unit, by enabling a node using “qsub -I -X, module load app/ANSYS, cfx5solve” and opening the file as a running simulation. This step is optional.

IV. POST-PROCESSING

Post-processing involves the analysis of the results and calculation of derived-data

In aerodynamics, all of the derived data, including the lift force (L), drag force (D), and the aerodynamic coefficients, depend on the pressure and velocity; therefore, these two variables are some of the most important factors to evaluate using the graphical tools

A. OVERVIEW

The creation of different graphical aids in Ansys CFD-Post and the resulting interpretation of the physical variables, such as velocities and pressure are discussed in this chapter. Also, the section covers the process of determining the accuracy of the physics calculated in the boundary layer over the wing surface.

B. CONVERGENCE CRITERION

Convergence can be defined as the characteristic of a function that approaches to a target value as the independent variable increases or decreases its value. In CFD, the convergence is analyzed to evaluate the fidelity of simulation results. In [14], it is explained that convergence depends on two factors: consistency and stability. The first property establishes that the truncation error needs to approach zero when all the differences of time and/or space tend to zero. The stability property indicates a solution that does not magnify the errors involved in the numerical simulation, avoiding divergent solutions.

The convergence can be viewed during the iterative process in the CFX-Solve GUI using the display monitors. The consistency convergence test is to observe that the residual target used by the software is met the behavior of the iterative process (Figure 26):

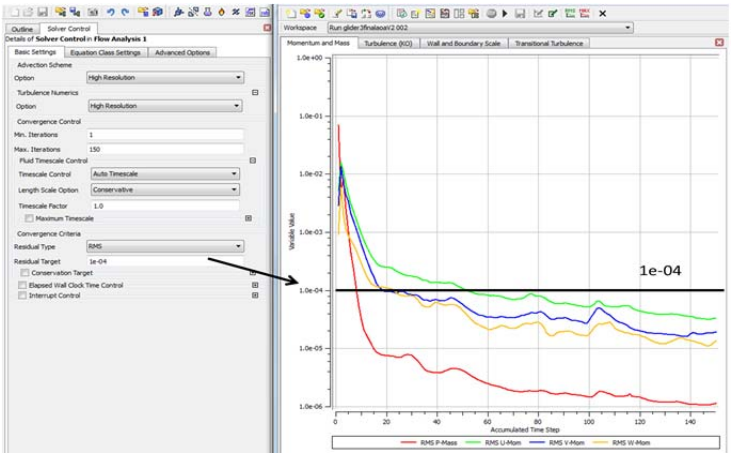

Figure 26. Residual Momentum and Mass Monitor of the SBXC Glider at 12 m/s with 3 Degrees AoA Matching with the Residual Target. Based on [14].

A good approach to develop a stability test is to monitor a physical value like forces. The goal is to observe asymptotic behavior in the reported variable value. For example, the tangential force in the X direction is shown in Figure 27. Doubling the number of iterations and corresponding CPU time only changed the force in X direction by about 1%; therefore, 100 iterations was demand acceptable.

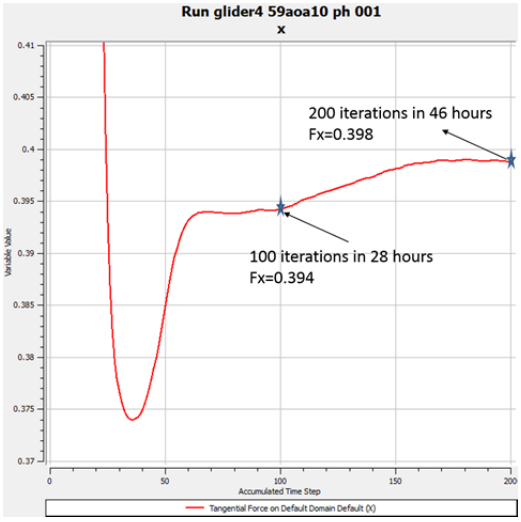

Figure 27. Residual Tangential Force in X Direction Monitor of the SBXC Glider at 12 m/s with 4.59 Degrees AoA for 200 Iterations.

1. Common Errors during the CFD Process

A concern in CFD is the loss of accuracy due to poor meshing process, solver setting, and the setup of the boundary conditions; therefore, it is important to understand and take care of the grid construction, solver and BC settings.

a. Grid Convergence

The grid convergence, also known as grid independence, is one of the common evaluations in CFD to manage errors. The first step of the process is to mesh the fluid domain, run a simulation, and analyze the consistency and stability of the solution; next, refine the mesh by reducing the size and angle of curvature and re-run the simulation. If the two solutions are close enough, then the user has achieved the grid independence.

This part of meshing can sometimes be a lengthy process, but is essential to assure the quality of the mesh is not adversely affecting the results. In Figure 28, an improvement of the accuracy can be observed for similar solutions using two different meshes.

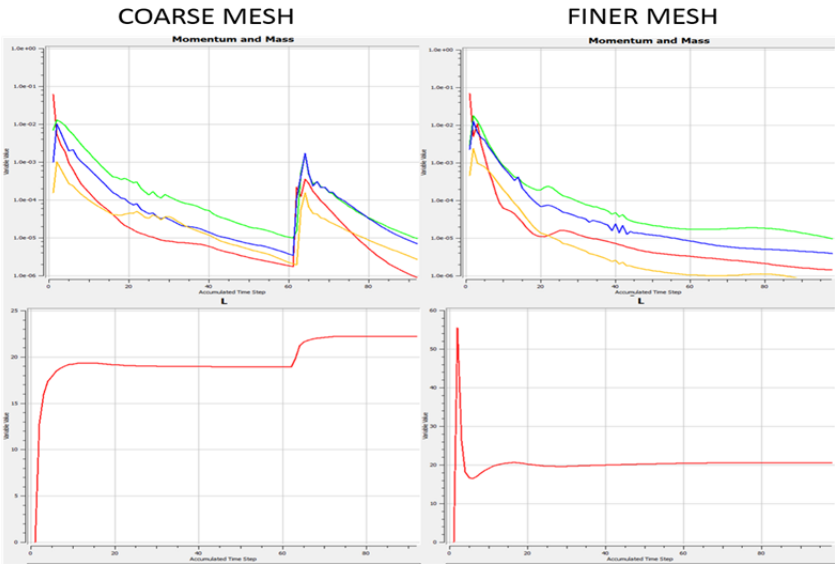

Figure 28. Consistency and Stability Comparison between Two Different Quality Meshes for the SBXC Wing at 12 m/s at 3 Degrees AoA at 100 Iterations.

2. User Error

There are plenty of potential sources of user error during the CFD procedure, such as poor geometry modeling, incorrect boundary conditions, and non-optimal solver setup. The consequences can appear during the meshing process (Figure 29), during the iterative solution process or at the end when the desired convergence cannot be achieved.

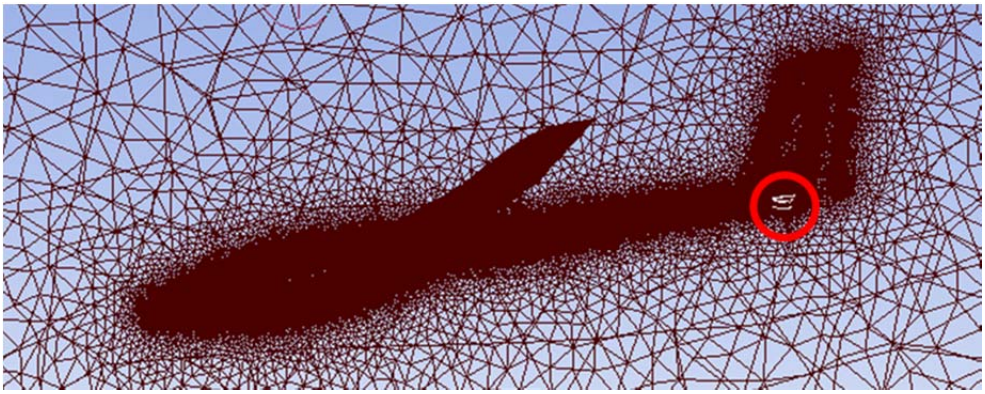

Figure 29. Mesh Failure Due to Bad Geometry Construction of the SBXC Airframe.

Based on the size of the mesh, a larger number of partitions were needed to allow the Ansys-Solver algorithm to process the task. A constant error appeared during the running preparation (Figure 30), indicating that the software required a certain amount of memory. After modifying the partitions parameters from Metis to Optimized Recursive Cord Bisection, the software was able to simulate meshes with more than 20 million nodes.

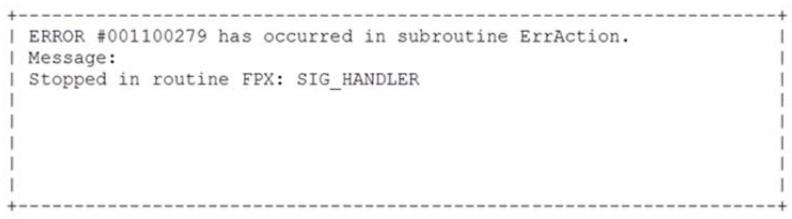

Figure 30. Sig Handler Error Due to a Wrong Selection of Partition Method.

This is a perfect example of user inexperience that caused a waste of computational resources and analysis time, forcing the user to run a lower quality mesh with less accurate results.

3. Residual Error

Chapter V of [14] discusses the two principal residual error sources. The first one is the application of large residual targets and the second one is the intolerance of the user to wait until the stability of the solution is achieved. The first case allows the CFD-Solver algorithm to end the simulation far away from the convergence status, and the second case can be achieved by interrupting the iterative process before the stability status can be clearly observed or when the user only requested a low number of iterations with the intention to accelerate the simulation. During the development of this thesis, several amounts of simulations were performed to recognize that the residual target has to be set to of $1x10^{-5}$ to avoid the sudden ending of the simulation and the physical value of tangential force in X direction and normal force in Y direction had to have a difference at least of $1x10^{-03}$ in a range of 50 iterations.

C. YPLUS VALUE

The y^+ value (Y plus) is a non-dimensional number that indicates the region from the wall where the different fluid states occurs [24]. In boundary layer theory, there are three important zones to be considered (Figure 31); the laminar region, the transition region and the turbulent region. For high Reynold numbers flows, the laminar and transitional regions might be very short and potentially ignored, but for low Reynold numbers flows, like this study, they are very important.

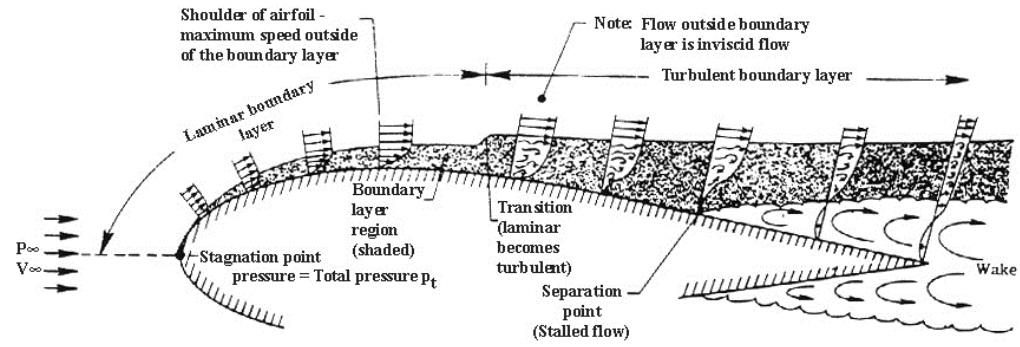
Shoulder of airfoil - maximum speed outside of the boundary layer
Note: Flow outside boundary layer is inviscid flow
Turbulent boundary layer
Laminar boundary layer
Boundary layer region (shaded)
Transition (laminar becomes turbulent)
P∞
V∞
Stagnation point pressure = Total pressure p_t
Separation point (Stalled flow)
Wake

Figure 31. Boundary Layer Separation Over an Airfoil. Source: [25].

A primary interest of this research is to resolve the boundary layer phenomena to predict, principally, the drag force on the SBXC glider; therefore, the major effort is to accurately resolve the viscous sublayer around the wing (Figure 32):

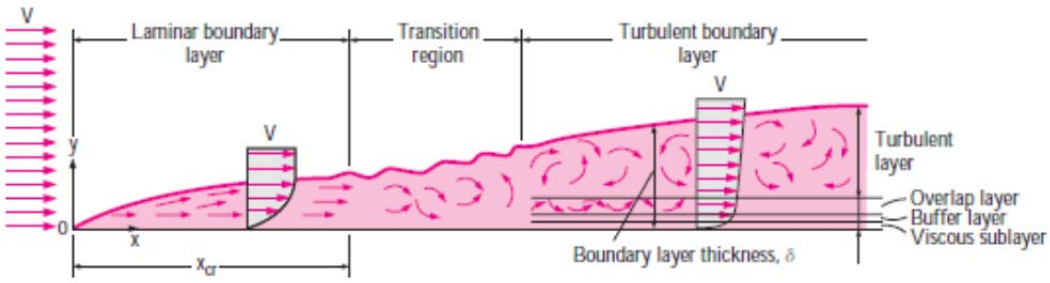

Figure 32. Development of the Boundary Layer for Flow Over a Flat Plate and the Different Flow Regimes. Source [26].

The acceptable range of first layer y^+ *to* get an accurate turbulent boundary layer solution is between 1–5, but experienced CFD users usually recommend values less than or equal to 1 at least in the turbulent region (Figure 33):

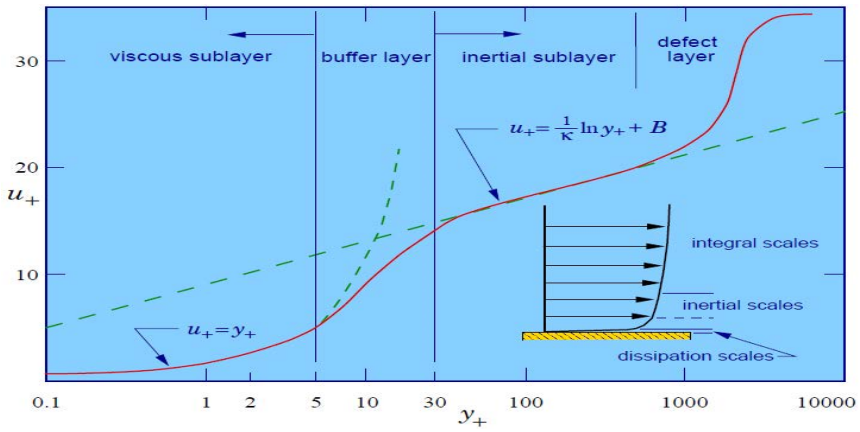

Figure 33. y^+ Range between Flow Regimes. Source: [24]

A good way to approximate the first layer mesh thickness (first wall distance) to assure a desired value of y^+ is by calculating it based on the following equations: Reynolds number, y^+, frictional velocity, and wall shear stress with external skin friction factor (Equations 4.1, 4.2, 4.3 and 4.4, respectively).

$$\mathrm{Re} = \frac{\rho U_\infty \mathrm{C}}{\mu} \tag{4.1}$$

$$y^+ = \frac{\rho U_\tau \Delta_{y1}}{\mu} \tag{4.2}$$

$$U_\tau = \sqrt{\frac{\tau_w}{\rho}} \tag{4.3}$$

$$\tau_w = 0.5 \mathrm{C}_f \, \rho U_\infty{}^2 ; @ \mathrm{C}_f = 0.058 \mathrm{Re}^{-0.2} \tag{4.4}$$

Where *Re* is the Reynolds number, ρ is the density of the air, U_∞ is the freestream velocity, U_τ is the friction velocity, *C* is the chord length of the root profile of the wing; μ is the dynamic viscosity of the air, Δ_{y1} is the first layer thickness, τ_w is the wall shear stress, and C_f is the skin coefficient friction for external flows.

By solving Equation (4.2) for Δ_{y1} and using the root chord length of the SBXC (0.3 meters) at 12 m/s, the first layer thickness obtained was 2.36 x10^{-05}.

Solving for Δ_{y1} gives the user an idea of the input required for the inflation method during the mesh process. Unfortunately, the y^+ final value can be analyzed only during post-processing, and sometimes a mesh refinement is required, as seen in Figure 34:

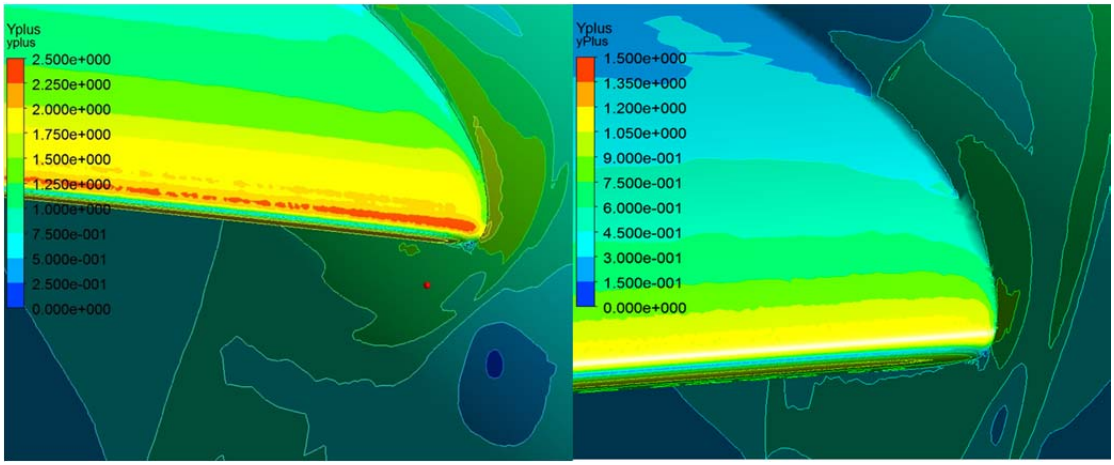

Left profile is a mesh with 2.36 x10^{-5} first layer thickness and right profile is a mesh with 1 x10^{-5} first layer thickness.

Figure 34. Comparison of y^+ between Two Different Values of First Layer Thickness for the SBXC Glider Fluid Domain.

Some recommendations to obtain the range of the desired of y^+ are:

- Create an accurate geometry during the fluid domain process.
- Use a small angle of curvature and/or sufficiently small min size during the meshing process.

With the final value on the wing surface obtained between 1 and 1.2., the meshing process methodology was accepted, and the solution obtained by the simulation can be trusted.

D. PRESSURE AND VELOCITY CONTOURS

During the Post-Process analysis, it is important to make sure the physics shown in the GUI make sense. Important variables to observe in aerodynamics are velocity and pressure; therefore, the application of tools such as contours helps the engineer to check the correct application of BCs and identify bad grid issues.

During the project development, two types of contours were analyzed: The first one was the body contour that helped to identify any discrepancy on the geometry model or any area where the meshing techniques were not applied correctly; the second one was the plane contour that assisted in identifying the basic points of interest for the aerodynamicist, including stagnation point, separated flow if present section, boundary layer regions, and also confirmation that the fluid domain size is sufficient.

Body pressure contours for the SBXC glider are shown in Figure 35, and indicates the lack of non-physical disturbances on the glider surface, especially on the wing. Also seen is the difference of pressure between the top and bottom of the wing surface pointing to a lift force generated. Finally, an important fact to note is the stagnation point indicated by the red color in the leading edge areas of the wing, horizontal stabilizer, vertical stabilizer and nose.

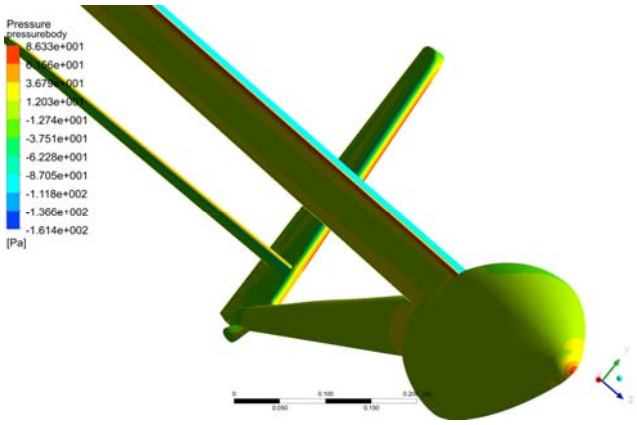

Figure 35. Pressure Body Contour of the SBXC Glider at 12 m/s at 4.59 Degrees AoA.

The plane contour technique was used to analyze velocity and pressure. In Figure 36, it is easier to identify the stagnation point and the difference of pressure in a specific section of the wing, helping to visualize the pressure zones over the airframe surface with the objective to verify the right size of the fluid domain by identifying high pressure zones in the corners and to assure the lift force generated on the body.

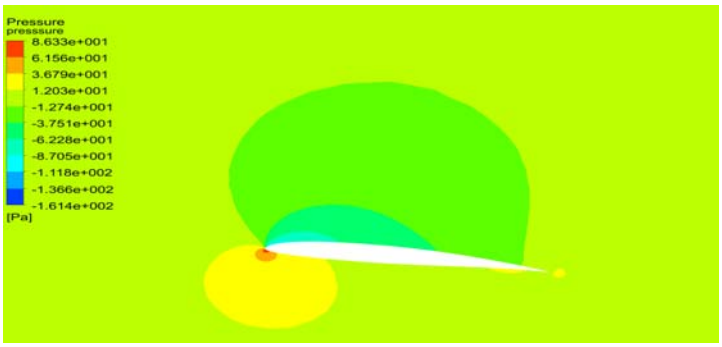

Figure 36. Plane Pressure Contour of the SBXC Glider at 12m/s with 4.59 Degrees AoA.

For the velocity analysis, the same technique was used. The limit of the boundary layer on a specific SBXC wing section located one meter away from the wing root is shown in Figure 37. The boundary layer can be found when the flow velocity reaches the 99% of the local outer flow velocity.

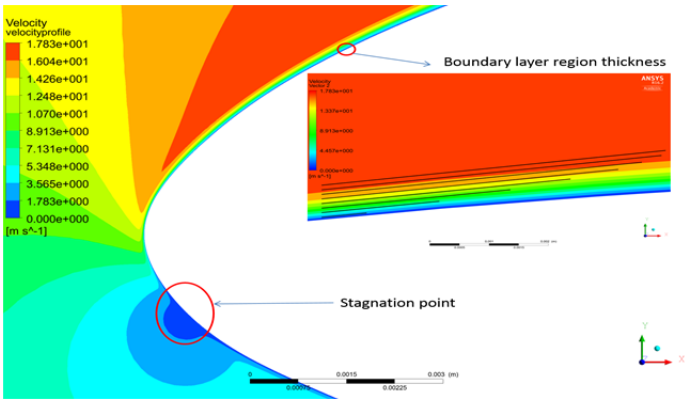

Figure 37. Boundary Layer Thickness for the SBXC Glider at 12 m/s with 4.59 Degrees AoA.

The velocity plane contour also indicates the separated region of the fluid from the surface near the trailing edge. To make the velocity analysis, the streamline and vector tool were used to complement the previous one. The edge of the boundary layer and the separation streamline of the air is shown in Figure 38. It can be clearly seen where the velocity vectors change directions and where the fluid velocity is completely developed. The fluid separation starts at 67.5% of the chord length at the section located at 0.34 meters from the wing root.

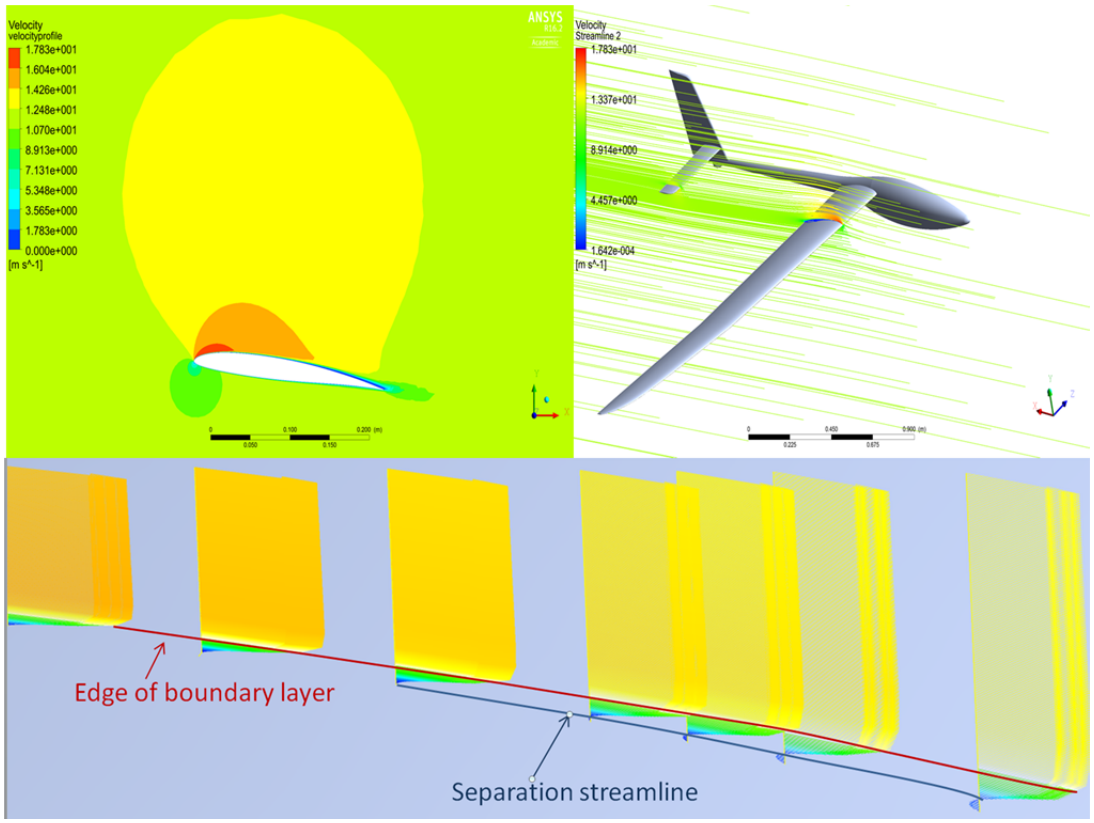

The analyzed section of the SBXC glider was located at 0.34 meters from the wing root.

Figure 38. Velocity Analysis of the SBXC at 12 m/s with 4.59 Degrees AoA.

An important feature verified in this thesis is the laminar behavior of the modified S2048. This process was done using the X wall shear around a wing section located at 0.44 meters from the wing root. Figure 39 shows the laminar

behavior of the airfoil. The negative values starting at 2/3 of the chord as is expected due to the separation over the last third part of the airfoil.

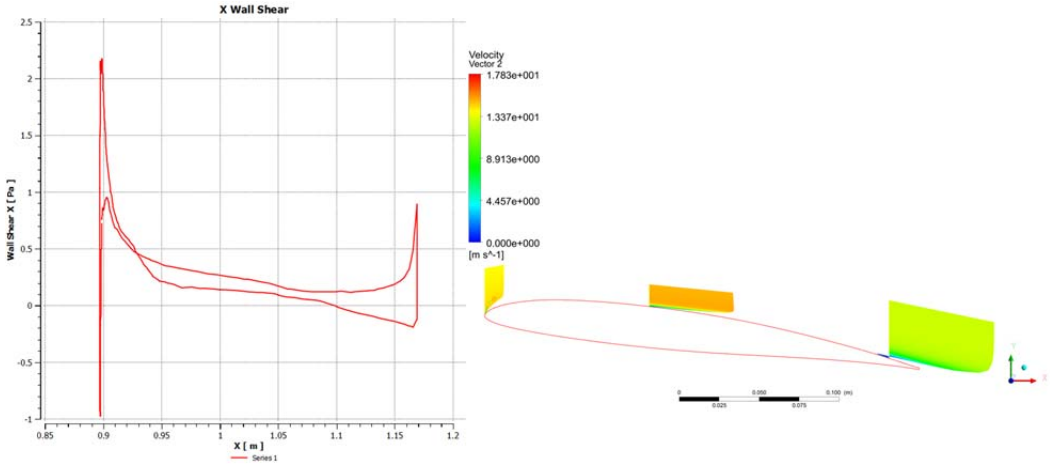

Figure 39. Wall Shear around a SBXC Wing Section.

E. DERIVED DATA

The derived data of interest from the simulation includes the coefficient of lift (Cl), coefficient of drag (Cd), and the sink polar data.

During the development of this project, different velocities were tested at different AoAs with the objective of finding the gliding flight condition where L matched the weight (W) and net drag was zero. The procedure was based on the equilibrium of forces acting on the glider and by making the assumption that the net drag force (D) is zero when gliding, using Figure 40 as a free body diagram to derive the Equations (4.5) and (4.6). It should be mentioned that net drag is equal to viscous drag plus pressure drag, where pressure drag is negative.

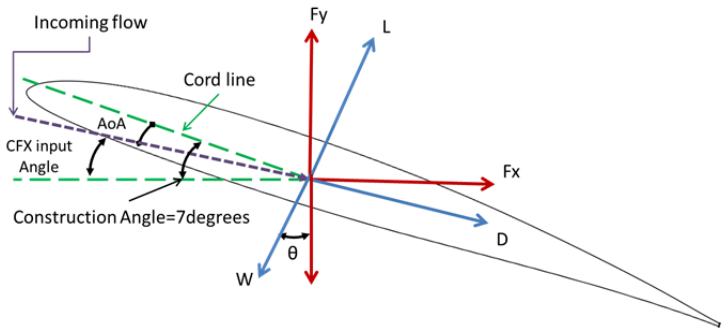

Figure 40. Free Body Diagram for the SBXC Equilibrium Analysis.

$$D = F_x \cos\theta - F_y \sin\theta = 0 \therefore \theta = \tan^{-1}\left(\frac{F_x}{F_y}\right) \tag{4.5}$$

$$L = F_y \cos(\theta) + F_x \sin(\theta) \tag{4.6}$$

The velocity range analyzed were from 10 m/s to 24 m/s, as indicated in Table 11. To obtain the value of lift force equal weight of 26.98N (5.5 kg of mass) for each velocity condition, it was necessary to evaluate at least 3 simulations with different AoAs; the first guess determined if it was necessary to increase or decrease the AoA; the second guess was used to estimate the behavior range of the lift force; and, the third simulation was done using an angle obtained using linear interpolation between the first and second guess (Figure 41).

Table 11. Range of Velocities Analyzed for the SBXC Glider.

		Guess1				Guess2					Linear interpolation					
Vel	AoA1	CFXA1	Fx1	Fy1	L1	AoA2	CFXA2	Fx2	Fy2	L2	AoA	CFXA	Fx	Fy	L	Dif.
(m/s)	(Deg)	(Deg)	(N)	(N)	(N)	(Deg)	(Deg)	(N)	(N)	(N)	(Deg)	(Deg)	(N)	(N)	(N)	(N)
10	8	1	0.838	26.73	26.74	8.5	1.5	0.71	27.88	27.89	8.105	1.105	0.805	26.95	26.962	0.0182
12	4	3	2.301	24.21	24.3	5	2	2.16	28.71	28.77	4.594	2.406	2.231	26.89	26.98	-0.0001
14	4	3	3.084	33.33	33.48	3	4	3.09	27.09	27.27	2.953	4.04	3.105	26.88	27.041	-0.0611
15	1.5	5.5	3.114	19.39	20.68	2.5	4.5	3.49	27.81	28.03	2.357	4.643	3.459	26.57	27.01	-0.03
18	1.5	5.5	4.541	30.44	30.44	1	6	4.22	25.32	26.66	1.129	5.871	4.308	26.65	27	-0.0204
21	0	7	21.22	4.519	21.7	0.3	6.7	4.92	25.97	25.97	0.372	6.628	5.008	26.49	26.962	0.0179
24	1	6	7.412	46.74	47.33	0	7	5.65	26.93	27.51	-0.12	7.119	5.67	26.26	26.864	0.1155

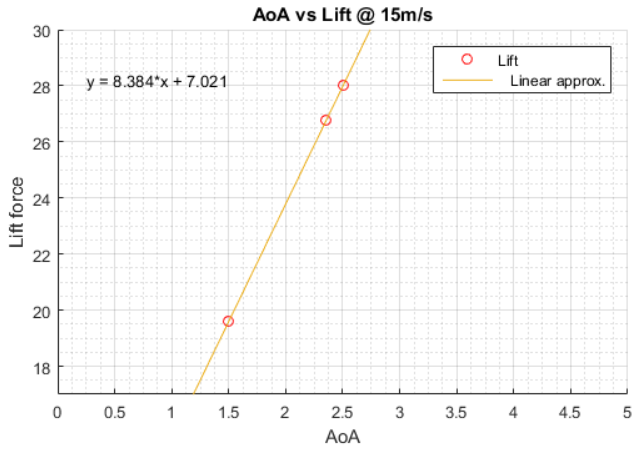

Figure 41. Linear Approximation Technique at 15 m/s for the SBXC Glider.

It is important to note that as the AoA increases, the CFX input angle (CFXA) decreases; therefore, the real model of the SBXC glider obeys the mathematical relationship shown in Equation (4.7):

$$CFXA + AoA = 7 \tag{4.7}$$

1. Coefficient of Lift and Drag

The lift and drag coefficient are calculated by dividing each force (*L, D* respectively) by the product of the dynamic pressure q_∞ and the wing area, *s* [27]. Equations (4.8) and (4.9) describe the dynamic pressure as the product of the density ρ times the square of the freestream velocity U_∞ divided by 2.

$$C_L = \frac{L}{q_\infty s} = \frac{L}{\frac{1}{2}\rho_\infty U_\infty^2 s} \tag{4.7}$$

$$Cd = \frac{D}{q_\infty s} = \frac{D}{\frac{1}{2}\rho_\infty U_\infty^2 s} \tag{4.8}$$

For the SBXC velocities analyzed, these coefficients were found using the CFX angle to solve the same equilibrium forces using the free body diagram of

the Figure 40 and eliminating the assumption of *D=0*. The results of each case are shown in Table 12, and the Cl and Cd plot for 18 m/s is shown in Figure 42. For the other velocities, the coefficients plots can be done using the same procedure.

Table 12. Cl and Cd Table for the Velocities Analyzed in the SBXC Glider Computer Model.

			Guess1					Guess2						Linear aproximation					
Vel (m/s)	q*s (N)	AoA1 (Deg)	CFXA 1 (Deg)	L1 (N)	D1 (N)	Cl1	Cd1	AoA2 (Deg)	CFXA 2 (Deg)	L2 (N)	D2 (N)	Cl2	Cd2	AoA (Deg)	CFXA (Deg)	L (N)	D (N)	Cl	Cd
10	39.95	8	1	25.66	1.173	0.642	0.029	-0.5	7.5	26.91	1.24	0.657	0.03	8.105	1.105	26.929	1.324	0.947	0.0466
12	40.95	4	3	26.96	1.1	0.658	0.027	5	2	28.77	1.156	0.703	0.028	4.594	2.406	26.958	1.1	0.6584	0.0269
14	55.73	4	3	33.45	1.335	0.6	0.024	3	4	27.24	1.197	0.489	0.021	2.953	4.04	27.034	1.2	0.4851	0.0215
15	63.98	1.5	5.5	19.6	1.241	0.306	0.019	2.5	4.5	28	1.295	0.438	0.02	2.357	4.643	26.763	1.297	0.4183	0.0203
18	92.13	1.5	5.5	30.73	1.602	0.334	0.017	1	6	25.62	1.547	0.278	0.017	1.129	5.871	26.955	1.559	0.2926	0.0169
21	125.4	0	7	21.62	1.898	0.172	0.015	0.3	6.7	25.9	1.909	0.207	0.015	0.372	6.628	25.896	1.917	0.2145	0.0152
24	163.8	1	6	26.76	2.372	0.163	0.014	0	7	27.41	2.324	0.167	0.014	-0.12	7.119	47.262	2.485	0.2886	0.0152

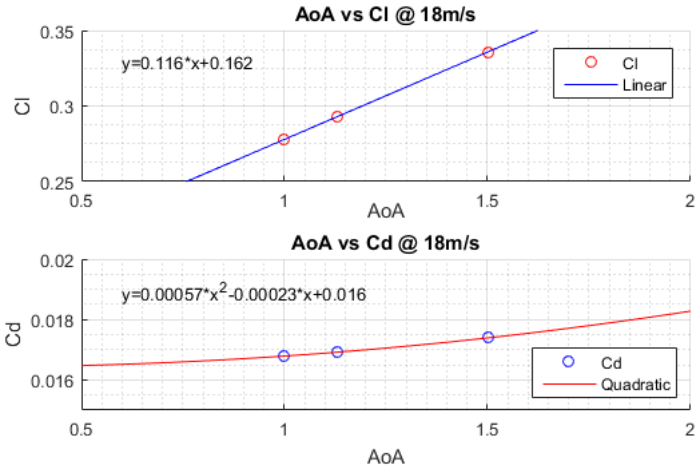

Figure 42. Cl and Cd Trend Lines for the SBXC Glider at 18 m/s.

2. Sink Polar

The sink polar or speed polar is a graphical representation that describes the gliding performance of the aircraft using the velocity of the air decomposed

into a vertical component called sink velocity, $V_{s,}$ and a horizontal component known as horizontal velocity, V_h [28].

For the SBXC analysis, the approach used to calculate the velocity components is based on the relationship shown in Figure 43 and Equation (4.9) that describes the Gliding Angle (*GA)*:

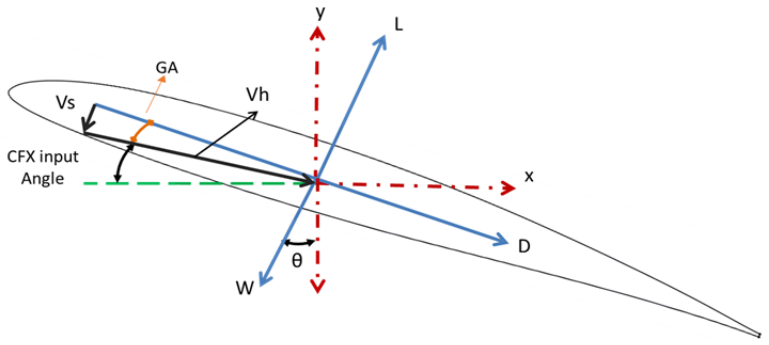

Figure 43. GA Relationship for the SBXC Model.

$$GA = \theta - CFXangle \tag{4.9}$$

Having GA, the values of V_h *and* V_s can be obtained using Equations (4.10) and (4.11), also the velocities components ratio is equal to the L/D ratio shown in Equation (4.12).

$$V_h = V\cos(GA) \tag{4.10}$$

$$V_s = V\sin(GA) \tag{4.11}$$

$$\frac{L}{D} = \frac{V_h}{V_s} = \cot(GA) \tag{4.12}$$

For the range of velocities analyzed, the values for GA and L/D ratio are shown in Table 13:

Table 13. L/D and Velocities Components.

Velocity	Theta	CFXA	GA	L/D	Vh	Vs
10	1.71	-1.1	2.815	20.33	9.98	-0.49
12	4.74	2.41	2.3376	24.5	12	-0.49
14	6.59	4.05	2.543	22.52	14	-0.62
15	7.35	4.64	2.714	21.1	15	-0.71
18	9.18	5.87	3.309	17.3	18	-1.03
21	10.7	6.63	4.077	14.03	21	-1.49
24	12.2	7.12	5.064	11.28	23.9	-2.12

The speed to fly, for max range, which means the gliding speed where the sink and forward velocity is the most beneficial, can be obtained by drawing a tangent line from the origin that is tangent to the sink polar curve, where the best L/D is located. Figure 44 shows the max value of L/D ratio and the corresponding V_h:

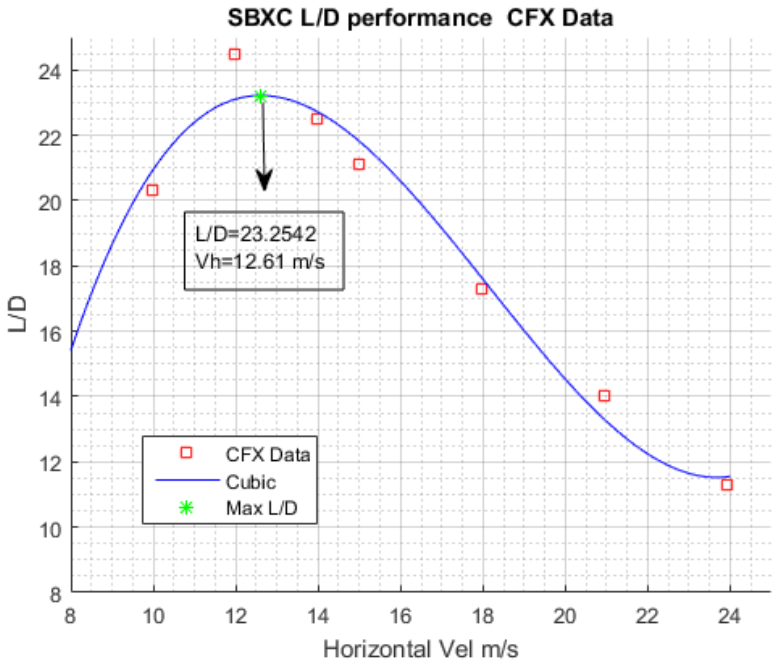

Figure 44. L/D Performance of the SBXC Glider Using CFD Technique.

After finding the maximum L/D value, the next step is to plot the sink polar curve using the velocity components and verify the L/D best value by plotting a tangent line from the origin of the coordinate frame. Other important information that can be obtained from the sink polar plot is the sink velocity for maximum endurance that is located where the minimum V_s is placed (Figure 45):

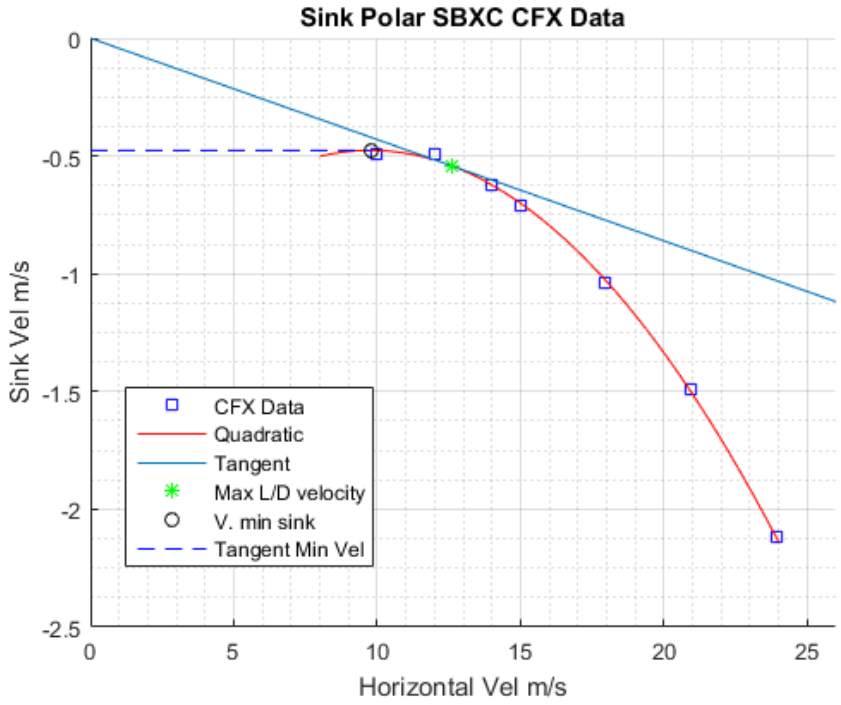

Figure 45. Sink Polar for the SBXC Glider Using CFX.

The quadratic curve fit for the computed for the sink polar curve for the SBXC Glider using CFD is shown in Equation (4.13):

$$V_s = -0.0082 * V_h^2 + 0.16 * V_h - 1.3 \tag{4.13}$$

The free-stream velocity is calculated based on the best L/D and minimum velocity components using Equation (4.14) based on the Pythagorean Theorem and the GA, using Equations (4.10) and (4.11).

$$V = \sqrt{V_h^2 + V_s^2} \tag{4.14}$$

The final results are shown in Table 14:

Table 14. SBXC-CFD Min and Best L/D Velocities Values and Derived Data.

	Vh (m/s)	Vs (m/s)	V (m/s)	L/D	Gliding Angle
Velocity for min sink.	9.77	-0.476	9.782	20.52	2.79
Velocity for max L/D.	12.61	-0.543	12.622	23.26	2.46

THIS PAGE INTENTIONALLY LEFT BLANK

V. RESULTS AND COMPARISON WITH REAL FLIGHT DATA

The simulation of physics phenomena helps the engineer to run many experiments of specific tasks without spending consumable materials avoiding safety risks, and saving time and money, but only if the computer model is accurate enough to describe the physics correctly.

This section compares the real flight test data from Edwards [12] and Ellias [11] with the computer model of the SBXC Glider using CFX techniques developed in this thesis. It has to be mentioned that the aircraft weight of the apparatus are different; the results shown in Edwards are scaled to 4.48 Kgs found in Ellias's data, and during the CFD analysis, the weight was assumed to be 5.5 Kgs based on the NPS Taleuas glider.

Figure 46 shows almost an identical shape in both cases; the only difference is the displacement to the right of the CFD model due to the higher horizontal velocities required for the heavier weight.

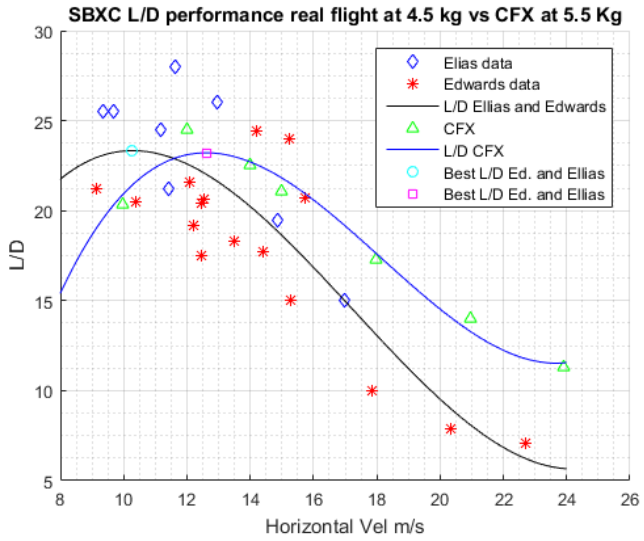

The values for the best L/D for their respective velocities are 23.33 for Ellias-Edwards data and 23.25 for the CFD analysis

Figure 46. L/D Performance of the SBXC Glider Using Real Data Flight and CFX Techniques.

The next step is to compare the sink polars. Equation (5.1) is a quadratic fit to the real flight data and Equation (4.13) is a quadratic fit to of the CFD analysis:

$$V_s = -0.019 * V_h^2 + 0.38V_h - 2.4 \tag{5.1}$$

The comparison between Equations (4.13) and (5.3) shows that the CFX data behaves similarly to the real flight data, the coefficient signs are the same, but the big difference is the first term coefficient that differs by a factor of roughly 2.

A big discrepancy is seen in Figure 45 between the sink polars for velocities are greater than about 15 m/s. Several potential causes that could affect the CFX data are:

- No consideration of the trim conditions as real flight data did
- No consideration of the surface details in the CFX model

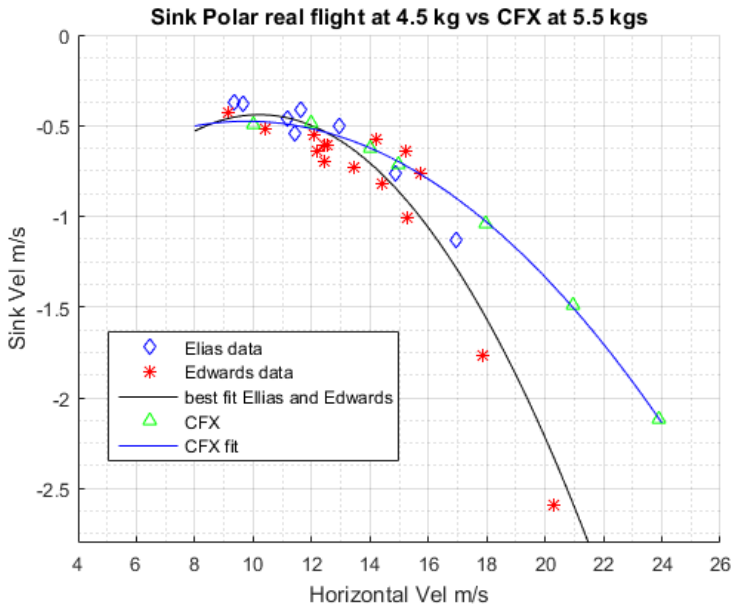

Figure 47. Sink Polar Comparison between Real Flight Data and CFX Analysis.

Based on [28], when the wing loading is different, the sink polar can be obtained using the ratio of the square roots between new weight and the reference weight as a scaling factor (Equation 5.2).

$$ScalingFactor = \sqrt{\frac{Wnew}{Wbase}} \tag{5.2}$$

Where *Wnew* is related to the 4.48 kilograms from the real flight data and *Wbase* based on 5.5 kilograms NPS TaLEUAS aircraft weight. Using equation 5.2, the scaling factor for the CFX analysis data is 0.90 and the comparison for the obtained data is shown in Table 15.

Table 15. Comparison Data between Real Flight and CFX Data.

Real Data Flight (Edwards-Ellias)					
	Vh (m/s)	**Vs (m/s)**	**V (m/s)**	**L/D**	**GA**
Vel. Sink min.	10.21	-0.44	10.22	23.20	2.468
Vel. Max L/D	10.28	-0.44	10.29	23.33	2.451
CFX Analysis Scaled Data					
	Vh (m/s)	**Vs (m/s)**	**V (m/s)**	**L/D**	**Gliding Angle**
Vel. Sink min.	8.82	-0.42	8.83	20.517	2.790
Vel. Max L/D	11.38	-0.49	11.39	23.254	2.462

The important fact to note is the region of minimum velocity and best L/D velocity, both techniques agree in the same region having the similar ratio for different weights and velocities.

Finally, the best L/D ratio obtained during real flight and simulations based on the free stream velocities used are listed in Table 16, where the similarity of the values between three methods can be observed:

Table 16. Best L/D for All the Methods Using the Free Stream Velocity without Fitting a Polynomial.

Method	Free stream Velocity (m/s)	Best L/D
Ellias	12.96	26
Edwards	11.308	24.4
Ansys-CFX	12	24.498

VI. CONCLUSIONS AND FUTURE WORK

This thesis implemented the Ansys-CFX configuration necessary to develop aerodynamic analysis of the SBXC airframe utilized in the TaLEUAS project at NPS with the main objective to simulate real flight data behavior. It should be mentioned that the 5.5 kg target weight was initially considered to help produce data suitable for the use in a simulation environment for the NPS fleet.

The research covered disciplines such as mechanics of fluids, numerical analysis, and computational fluids dynamics.

A. CONCLUSIONS

From the CFX data analysis, individually and in comparison with the real flight data, it was verified that the process of simulating the aerodynamics of the glider is achievable in the regions of U_∞ between 10 m/s and 15 m/s, but requires the following considerations to have better accuracy in the method for higher velocities:

- Possibly addition of a base drag coefficient by considering the small details in the airframe model that can produce disturbances in the fluid behavior such as control servos, controls surfaces gaps, and push rods.
- Considering trim conditions.

This first attempt to develop an aerodynamic analysis for the full SBXC airframe allowed the finding of the optimal velocity to fly and the minimum velocity to develop a TaLEUAS mission.

An important fact to emphasize is that the CFD methodology can be used as an important tool to design glider airframes and to extract a high fidelity approximation of the behavior of the body prior to construction. This technique can also be applied to analyze existing models with the objective to improve them.

Finally, this thesis also developed an easy procedure that allows aerodynamics students to follow step-by-step during the procedure of creating the fluid domain, selecting the right type of mesh, knowing how to analyze it, and inserting the boundary conditions correctly.

B. FUTURE WORK

The next step is to increase the accuracy of the glider model by adding control surfaces and taking the larger surface defects into account and by including trim-conditions like the stabilizer angle for zero moment.

An important additional step on this technique is to utilize CFD analysis with the objective of developing system identification. This could probably be done using an inviscid environment where the user would be able to obtain the control derivatives ready to be implemented in the control algorithm developed by TaLEUAS Project.

Finally, based on the necessities of the project and due to the constant actualization of the airframes, this thesis recommends the optimization process of the SBXC airframe based on the CFD analysis and the flight requirements.

Appendix. Solidworks-ANSYS-Hamming Simulation Process Gouge for Aerodynamics Analysis of the SBXC Wing

NOTE: A large number of files and folders were created during the simulation process; it is necessary to not use spaces in the names of the files or folders to avoid problems in the communication between software.

- Create a folder in your computer hard drive.
- Open Solidworks;
- In the Solidworks banner select: File, New, Part, and OK.
- In the Solidworks banner select: Tools, Options, Document properties-Units, Document properties, Units, Unit system, MMGS (millimeter, gram, second).
- Features, Reference geometry, Plane, First reference-select Front plane from the operations tree, Parallel, in distance one type 500 mm.
- Repeat plane step for distances of 1000 mm, 1500 mm, 2000mm, 2100 mm, 2190 mm. Each plane belongs to an airfoil section.
- Features, Curves, Curves through XYZ points. Browse "Section1.txt," click open and then OK.
- Repeat curve process for the missing sections until you complete all the wing structure.
- Create a sketch in the front plane; use the Spline and match all the points for the front plane airfoil. Use only one spline section starting from the leading edge in counterclockwise direction.
- Repeat the matching point process until you complete all the wing structure.
- To create the guide curves to match the shape of the wing, go to Features, Curves, Curve through reference points, then select parallel points of the leading edge until all the airfoils sections are touched (at least from the mid wing to the tip) to avoid deformation during the creation of the solid (Figure 48).
- Create as many guide curves as needed.
- Repeat the process for the trailing edge.

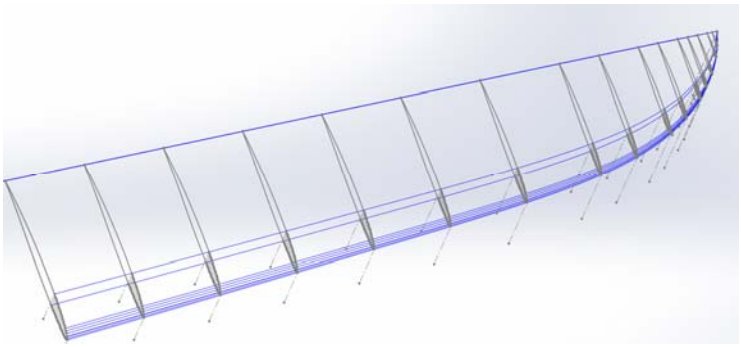

Figure 48. SBXC Mid Wing Section Structural View. Airfoil and Guide Curve Process.

- When the entire wing sections are connected by guide curves, a loft operation is required to form a solid figure. Go to Features, Lofted Boss/Base, Profiles-select the root profile (Section 1) up to the mid wing profile, Guide curves- select the curve that touches the leading edge and trailing edge between the airfoils sections. Checkmark Merge Tangent Faces option.

- Repeat the process for the missing sections. As a suggestion, do not select more than 5 airfoil sections to avoid deformations in the solid, and in the tip section try to do loft operations with only two profiles. At the end of the process, all the airfoil sections should be covered by the loft instruction creating a solid wing (Figure 49):

- Save the wing file, and do not close the file.

- For the creation of the fluid domain, go to Solidworks banner and select: File, New, Assembly, OK.

- In the Property manager, Part/Assembly to insert-select the wing created and drags it into the Solidworks workspace.

- Select the root airfoil section and click normal view.

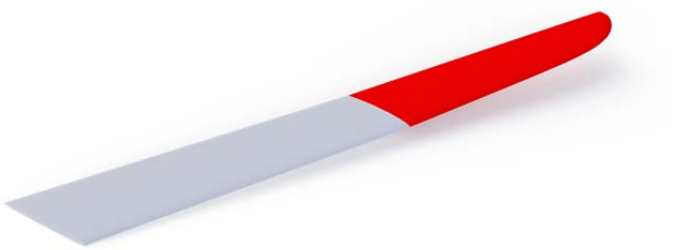

Figure 49. Solid SBXC Wing after the Loft Instruction.

- Select the root face of the wing and create a reference plane. Go to Assembly, Reference Geometry, Plane, Coincident. If the message in the property manager says “fully define,” click OK in the green check mark (Figure 50):

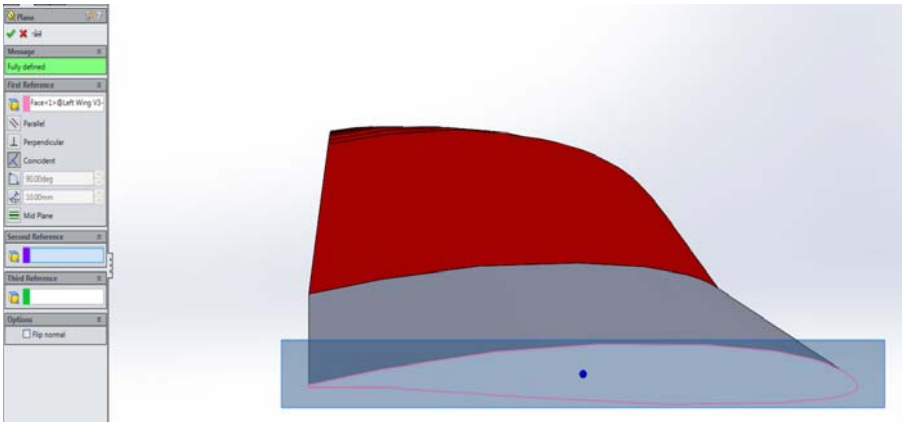

Figure 50. Creation of a Reference Plane in the Root of the Wing.

- Go to Assembly, Insert components, New part. Select the Plane1 created in the previous step from the Feature manager tree. Automatically, a sketch workspace is open.
- In the Sketch tab, select Line, Center line and draw a line from the middle of the leading edge to the middle to the trailing edge.
- In the Sketch tab, select center rectangle and grab the midpoint of the center line as a reference.
- Click in Smart dimension and input 4000 mm for the horizontal lines and 4000 mm for the vertical lines, and click OK.

- Go to Features, Extruded Boss/Base, select the direction to the tip of the wing by clicking the double arrow icon (only if it is necessary). In distance of Direction 1, type 4000 mm and click OK (Figure 51):

Figure 51. Extrusion Created with the Wing Inside. Both Solids Are Merged.

- In Solidworks Banner, go to Insert, Features, Cavity.
- Select the wing from the operations tree and then click OK in the green check mark. The fluid domain has been created (Figure 52).
- Right click on the new part created; open it, using the folder icon with the green arrow.
- Saved it as a separate file and also save it as a parasolid (*.x_t).

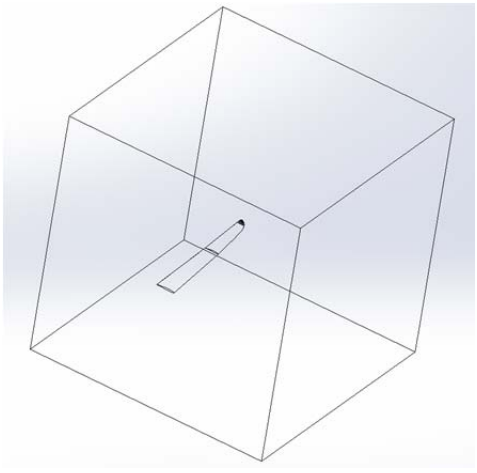

Figure 52. Wing Fluid Domain.

- Close Solidworks and open ANSYS workbench.

- From ANSYS toolbox, drag Fluid flow CFX to the Project Schematic area.
- Right click on the geometry tab of the CFX box; Import geometry, Browse and select the parasolid wing model (Figure 53).
- When the importation is done, a green check mark will appear next to geometry.
- Double click in mesh tab of the CFX box to open the mesh application.
- A solid fluid domain would appear in the mesh workspace. Click the Z axis to have a normal view or the wing root profile.
- Identify the orientation of the leading edge. In the Outline tree, right click on Model, then Insert, Name selection and name it as in listed in Figure 54.

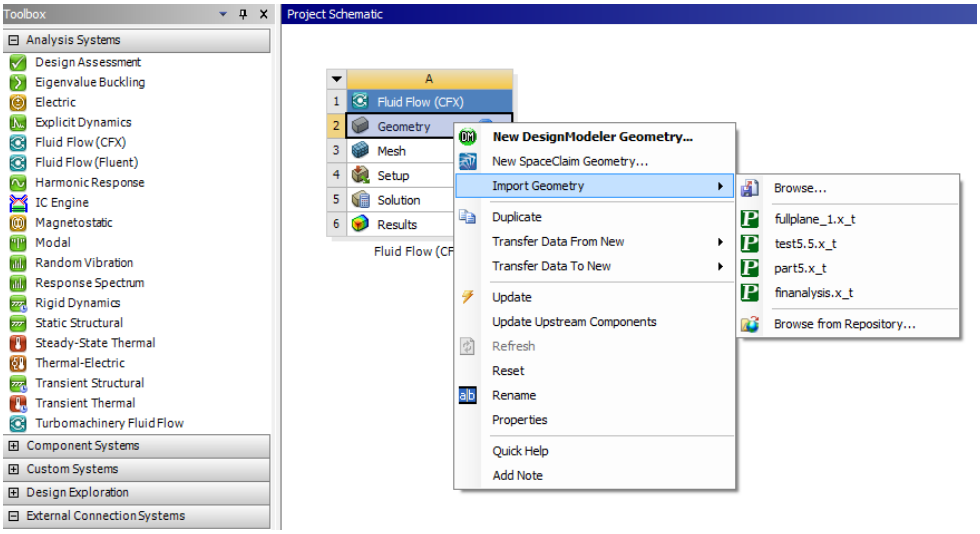

Figure 53. Import a Parasolid File to ANSYS CFX.

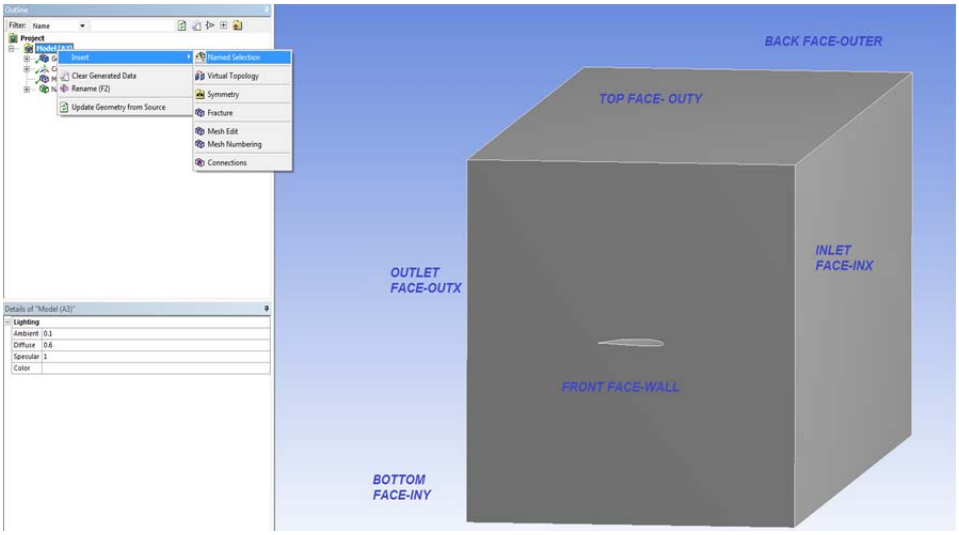

Figure 54. SBXC Fluid Domain, Named Selection Process.

- In the Outline tree, click mesh, then go to sizing under Detail of Mesh. In Use Advanced Sizing, select Proximity and Curvature. In Relevance Center, select Coarse; for Smoothing, select High, Transition Slow, Span Angle Center Fine, Curvature angle; type 1.5 degrees.

- For Min Size select 1 e -004 m, the others values for sizing can be considered as default.

- In the inflation Section, under Detail of Mesh, under Use Automatic Inflation, select Program Controlled. This function allows applying inflation in the wing body without using local control of the faces and would avoid applying inflation to named selection faces.

- Inflation option, select Last Aspect ratio, First Layer Height type 1.15 e-005 m. Maximum number of layers select 15, Aspect Ratio 1.25.

- Finally, click Generate Mesh. The end result should generate approximately 21 million of nodes and 57.4 million of elements (Figure 55).

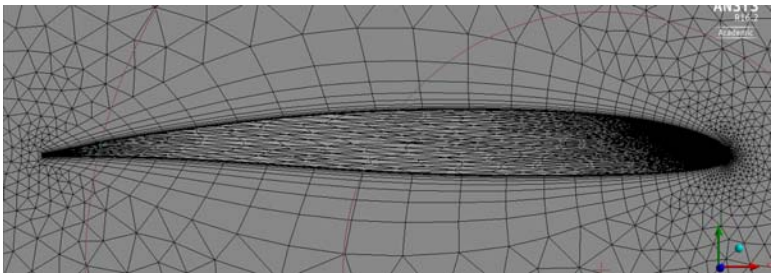

Figure 55. Mesh Generated for the SBXC Wing.

- It is important to double check the number of nodes due to the limitations of ANSYS partition algorithms. This information is necessary for the Hamming script.
- After the mesh is created, it is always a good idea to evaluate the quality of the mesh. Go to Statics, under Details of Mesh and, in Mesh Metric, select Element quality Statistics.
- A graphic representation of the quality of the elements appears under the mesh workspace. Click the bar between 0.25 and 0.38 element metric value and verify that the leading edge is between that ranges of element metrics. This test confirms the fidelity of the mesh and would support the simulation of the boundary layer in the leading edge. If the leading edge is below the range mentioned, refine the mesh (Figure 56):

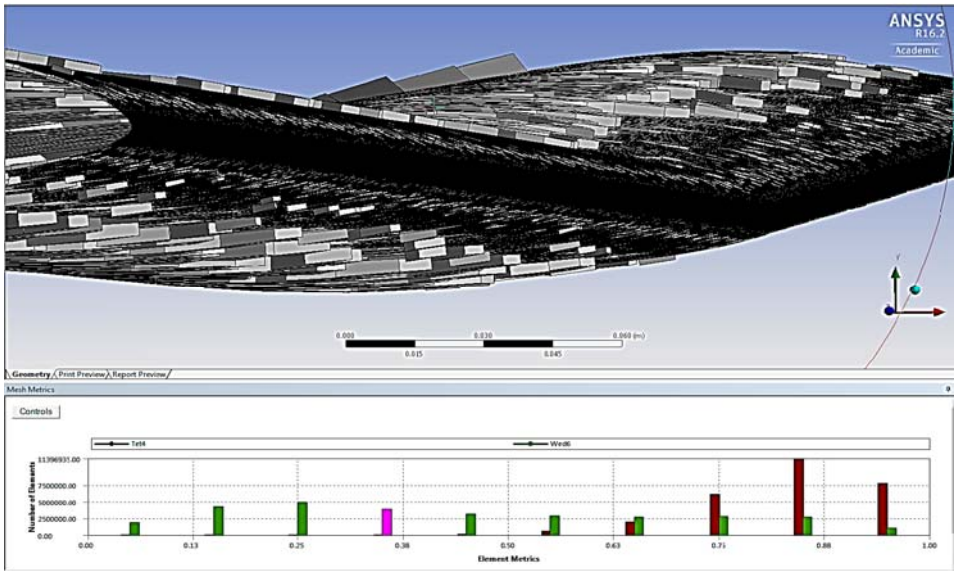

Leading is edge well define in metrics values 0.25 and 0.38.

Figure 56. Good Mesh Quality for the SBXC Wing.

- Close the mesh application, update the project in ANSYS project schematic, and save it. Wait until the recycle icon appears in the setup section in CFX box.

- Double click the setup option in CFX box to open CFX-Pre.

- Under Outline, double click on Analysis Type and verify that the Analysis Type is set to Steady State.

- Double click on Default domain, in Basic Settings.

Fluid and Particle definitions select Air a 25C with Continuous Fluid for morphology.

Domain Models, select 1 atmosphere for reference pressure and click apply.

- In Default domain, in Fluid Models:

Heat transfer, Isothermal with 25C Fluid temperature

Turbulence, Option= Shear Stress transport

Wall function= Automatic

Advanced Turbulence control; check transitional turbulence and select Gamma Theta Model, then click apply.

- Right click on Default domain; insert boundary. Name it INX.

Basic settings, Boundary Type= Inlet, Location= INX

Boundary Details, Option=Subsonic, Mass and Momentum, Option=Cartesian velocities components. U=-11.984, V=0.62803, W=0, Turbulence= Medium

Note: the U velocity sign will depend on the orientation of the ANSYS reference frame with respect to the leading edge. Also, this is a configuration for 12 m/s stream velocity at 3 degree angle of attack. Velocity components will change for other cases.

- Repeat the Inlet process for the face named INY. The velocity components are the same.

- Right click on Default domain, insert boundary. Name it OUTER.

Basic settings, Boundary Type= opening, Location= OUTER

Boundary Details, Option=Subsonic, Mass and Momentum, Option=Entrainment, Relative pressure= 0 pascal, Turbulence= Zero Gradient

- Right click on Default domain; insert boundary. Name it OUTX.

Basic settings, Boundary Type= Outlet, Location= OUTX

Boundary Details, Option=Subsonic, Mass and Momentum, Option= Static Pressure, Relative pressure= 0 pa

- Repeat the Outlet process for the face named OUTY.
- Right click on Default domain, insert boundary. Name it Sym.

Basic settings, Boundary Type= Symmetry, Location= WALL

- Compare the BC set up with Figure 57.

Note: Sometimes the cavity geometry is so complex or the parasolid model has some defects so that the symmetry plane is not recognized by ANSYS CFX. In this case, instead of Symmetry Boundary type, select Wall and in Boundary details, select Free Slip Wall for Mass and Momentum.

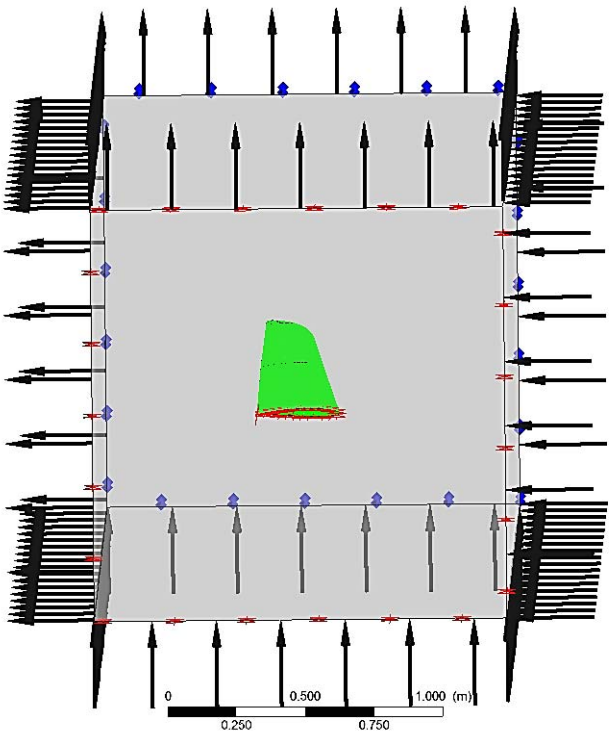

Figure 57. Boundary Conditions Applied to the SBXC Wing Fluid Domain.

- After the BCs are applied, double click on Solver control (under Outline-Solver).
- Basic settings, Advection scheme, Option= High resolution. Turbulence Numerics, Option= High resolution

Convergence Control, Max iterations 150

Residual target= 1e-05

- In Equations class settings, double check that the continuity, momentum, turbulence eddy frequency, and turbulence kinetic energy are in the equation class.
- In Advanced Options, make sure that Global Dynamic Model Control box is checked.
- Apply and save changes in the diskette icon. Close CFX-Pre, and update the project in ANSYS project schematic.
- Save your project and close ANSYS workbench.
- Open note pad text editor and create the following code shown in Figure 58:

#!/bin/bash
PBS cfx job submission script
#PBS -j oe
#PBS -N glider3finalaoaV2
#PBS -l walltime=48:00:00
#PBS -l nodes=1:ppn=16
#PBS -l pmem=8GB
#PBS -M agarciaa@nps.edu
#PBS -m abe
#!/bin/bash= defines a bash shell to be used.
PBS cfx job= defines the type of job to run.
PBS –N= enable identification name of the job.
PBS -l walltime= define the parallel computing time.
PBS –l nodes='x': ppn:'y'= define the numbers of nodes x and number of cores per node y.
PBS –l pmem= define the memory per core.
PBS –M= enable the user personal email.
PBS –m abe= send and email at beginning and at the end of the computing process.
#
echo some parameters
#
echo " "
echo "hostname = `hostname`"
echo "PBS_NODEFILE = $PBS_NODEFILE"
echo "JOB_ID = $JOB_ID"
echo "PBS_O_WORKDIR = $PBS_O_WORKDIR"
echo " "
echo "PBS_NODEFILE contents:"
echo "----------"
cat $PBS_NODEFILE
echo "----------"
Echo hamming parameters.
echo " "
source /etc/profile
module load app/ansys
export CFX5RSH=ssh
cd $PBS_O_WORKDIR
Enable Ansys application in hamming environment.
# Create hosts list
# echo par-dist = $(cat $PBS_NODEFILE)
PAR_LIST=$(sed -e '{:q;N;s/\n/,/g;t q}' $PBS_NODEFILE)
#
run the cfx job
#
cfx5solve -def glider3finalaoaV2.def -part-large -part-mode orcb -par-dist $PAR_LIST
#increase to large partition
Enable CFX-solve application,
select the definition and configure
A large partition with optimal recursive
method.
#-part-large
##-part-mode drcb
#-size-2 #this function help to increase memory allocation factor

Figure 58. Hamming Communication Script.

- Modify the necessary fields (identification name, email, and name of definition file, number of nodes and cores) as required.
- Save the file with extension *.sh. If the option is not available, just save it as a *.txt file and change the extension manually.
- Open MobaXterm_Personal_8.5 and login with your hamming account. If the software is not installed, download it from: http://mobaxterm.mobatek.net/download-home-edition.html, and configure your Hamming account.
- Create a folder for your jobs using the blue folder icon.
- Drag the script created into the new folder.

- Locate the ANSYS wing project; next, find the folder named *yourprojectname_files.* Open the folder, find a folder named dP0 and open it. Select the file called Fluid Flow CFX.cfx under the CFX folder, copy it and rename it with the same name used in the hamming script.

- Drag the *.cfx file into the folder created in Hamming (Figure 59):

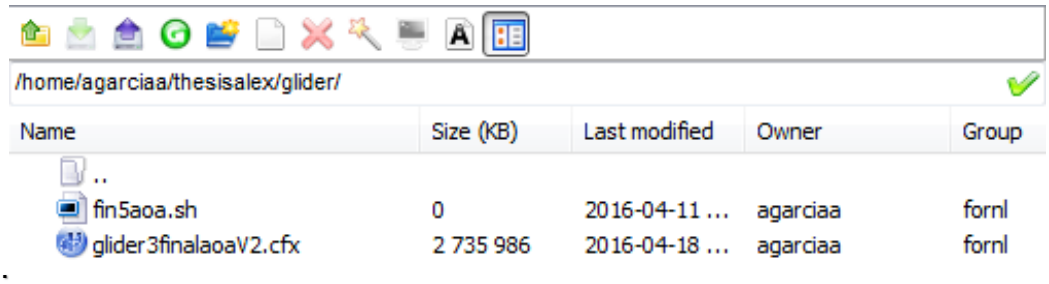

Figure 59. MobaXterm Window with Script and CFX Files.

- In Hamming command type:

qsub –I –X, to enable a node using the graphic interface

When the node is active, type **module load app/ANSYS.**

Next type **cfx5pre –gr mesa**, to open the CFX-Pre ANSYS application.

- In CFX-Pre, browse for the *.cfx file and open it.

- Create a definition file using the instruction called *write a solver input file* with a blue diskette and paper icon.

- Save your definition file with the same name used in the script and in the same location as the script and CFX file.

- Close the CFX-Pre application and go back to Hamming environment.

- In Hamming command type:

cd yourfoldername, to allow you to move to the named subdirectory.

Next, type **ls**, to identify all the documents are placed in the right folder.

Finally, type **qsub nameofyour*.sh file**, to submit the file to the cluster.

- An email will be sent to the user when the computation starts, and another email will be sent when the computation is over.

- In Hamming command window, type **cfx5solve** to open ANSYS solver application. Browse for the running file and open it. The user will identify the running file by the *.dir extension.
- Analyze the convergence of your simulation using the graphs and close the GUI.
- Wait until the computation is finished. Refresh your folder in Hamming.
- Locate the file with the extension *.res and save it in the hard drive of the local computer.
- In the computer, double click the *.res to open the CFD-Post.
- Once in CD-Post, the wireframe appears; Insert, Location, Plane.
- Under Details of Plane

Geometry, Definition, Method, XY Plane Definition, Z=-1 meter. Color, Mode, Variable, Velocity. Then apply (Figure 60).

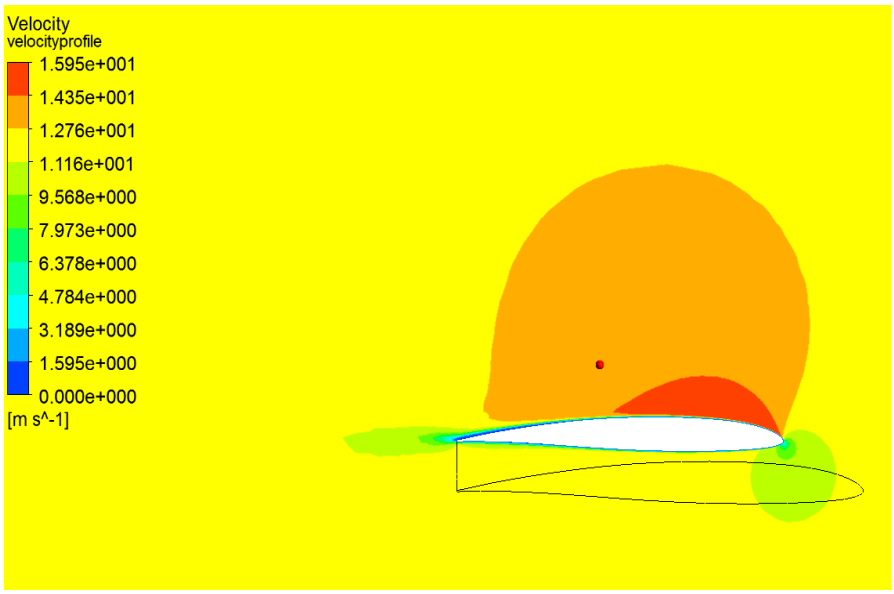

Figure 60. Velocity Profile Using Plane Instruction.

- Analyze the velocity profile, identify the max-min velocities areas and look for potential deformations in the profiles; also look for inconsistencies in the corners of the fluid domains.

- Repeat the plane process for a Pressure variable (Figure 61). Note: Only modify the variable option to Pressure if the same plane wants to be used and identify the stagnation point.

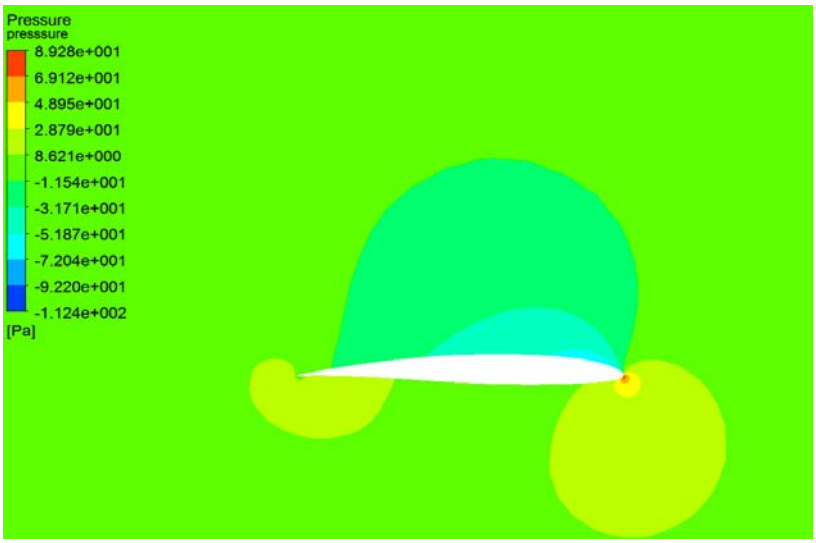

Figure 61. Pressure Profile Using Plane Instruction.

- Next, uncheck the plane boxes. Go to Insert, Contour and under Details of Contour

Geometry, Location=Default Domain, Variable=Yplus. Then apply

- Verify Yplus value on the leading edge. The range of values has to be between 0.9 and 1.15 (Figure 62).

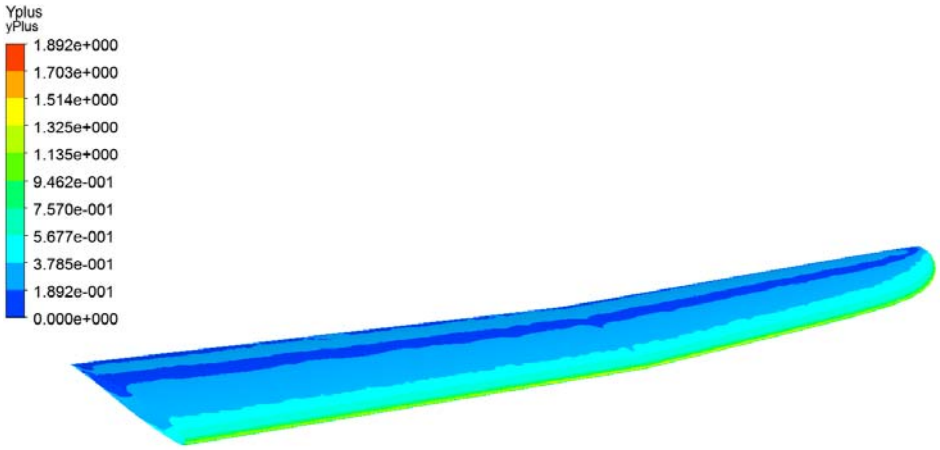

Figure 62. Yplus Body Profile Using Contours Instruction.

- Repeat the Contour process for a Pressure variable in the Default Domain and look for pressure irregularities on the wing surface, like an extreme value in a single spot (Figure 63).

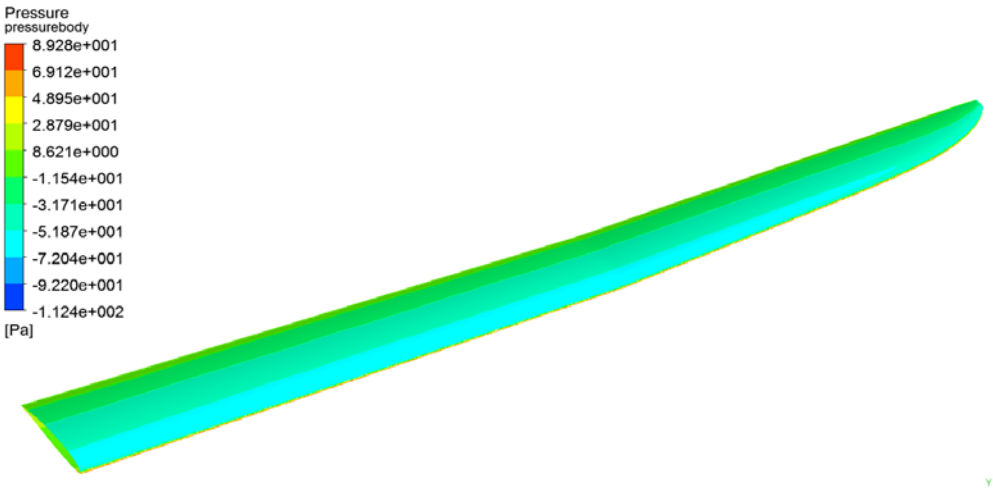

Figure 63. Pressure Body Profile Using Contours Instruction.

- Click on Function calculator (the icon of a calculator with a letter “f”; it is the fifth to last icon on the top bar).
- In function calculator

Function=Force, Location= Default Domain, Direction= Global X. Click calculate.

- The result of force in X should be close to 0.24 Newton.
- Repeat the process for the force in Y. The result should be approximately 20.5 Newton.

THIS PAGE INTENTIONALLY LEFT BLANK

LIST OF REFERENCES

[1] M. J. Allen, “Autonomous soaring for improved endurance of a small uninhabited air vehicle,” presented at 43rd AIAA Aerospace Sciences Meeting and Exhibit, Reno, NV, 2005.

[2] N. E. Kahveci and P. A. Ioannou, “A heuristic search algorithm for maneuvering of UAVs across dense thermal areas,” presented at AIAA Guidance, Navigation and Control Conference and Exhibit, Hilton Head, SC, 2007.

[3] D. J. Edwards, “Implementation details and flight test results of an autonomous soaring controller,” presented at AIAA Guidance, Navigation and Control Conference and Exhibit, Honolulu, HI, 2008.

[4] A. T. Klesh and P. T. Kabamba, “Solar-powered aircraft: Energy-optimal path planning and perpetual endurance,” *Journal of Guidance, Control and Dynamics*, vol. 32, no. 4, pp. 1320–1329, July 2009.

[5] K. Andersson, I. Kaminer, K. D. Jones, V. Dobrokhodov and D. J. Lee, “Cooperating uavs using thermal lift to extend endurance,” presented at AIAA Infotech Aerospace Conference, Seattle, WA, 2009.

[6] K. Andersson and I. Kaminer, “On stability of a thermal centering controller,” presented at AIAA Guidance, Navigation and Control Conference, Chicago, IL, 2009.

[7] K. Andersson, I. Kaminer and K. D. Jones, “Autonomous soaring; flight test results of thermal centering controller, “presented at AIAA Guidance, Navigation and Control Conference, Toronto, ON, 2010.

[8] N. Camacho, V. Dobrokhodov and K. D. Jones, “Cooperative autonomy of multiple solar-powered thermaling gliders,” presented at Proceedings of the 19th IFAC World Congress, 2014, Cape Town, SA, 2014.

[9] N. Camacho, “Improving operational effectiveness of tactical long endurance unmanned aerial systems (TALEUAS) by utilizing solar power,” M.S. thesis, Dept. MAE, Naval Postgraduate School, Monterey, CA, 2014.

[10] R. T. I. Fauci, “Power management system design for solar-powered UAS,” M.S. thesis, Dept. ECE, Naval Postgraduate School, Monterey, CA, 2015.

[11] J. Ellias, Performance Testing of RNR's SBXC Using GPS, [Online]. Available: http://www.xcsoaring.com/ techPicts/%20Ellias%20performance%20test.p df. Accessed 11 April 2016.

[12] D. Edwards, Performance Testing of RNR's SBXC Using Piccolo Autopilot," 14 March 2008. [Online]. Available: http://www.xcsoaring.com/ techpicts/edwards%20performance%20test.pdf. Accessed 10 April 2016.

[13] K. Y. W. and H. Bang, *The Finite Element Method Using Matlab*, Boca Raton, FL: CRC Press LLC, 2000, pp. 1–2.

[14] J. Tu, G. H. Yeoh and C. Liu, *Computational Fluid Dynamics: A Practical Approach*, Burlington, MA: Butterworth-Heinemann, 2007, pp. 4–8, 46-55,180-211.

[15] S. G. Kotogiannis and J. A. Ekaterinaris, "Design, performance evaluation and optimization," *Aerospace Science and Technology*, vol. 29, no. 1, pp. 339–350, August 2013.

[16] W. Jin and Y. G. Lee, "Computational analysis of the aerodynamic performance of a long-endurance UAV," *International Journal of Aeronautical and Space Sciences*, vol. 15, no. 4, pp. 374–382, December 2014.

[17] P. Panagiotou, C. Salpingidou, P. Kaparos and K. Yakinthos, "A CFD-AIDED design procedure, performance estimation and optimization study of MALE UAV," presented at 8th GRACM International Congress on Computational Mechanics, Volos, GR, 2015.

[18] M. Selig, Donovan and Fraser, *Airfoils at Low Speeds*, Virginia Beach, VA: H. A. Stokely, Publisher, 1989, pp. 72–73,113.

[19] "Rensselaer Polytechnique Institute," 13 March 2015. [Online]. Available: http://homepages.rpi.edu/~morrij5/CAD/Import_Points.pdf. Accessed 13 April 2016.

[20] Ansys, "Ansys meshing user's guide," Ansys, Canonsburg, PA, 2013.

[21] Ansys, "Lecture 5 Global Mesh Controls, Introduction to Ansys meshing," Ansys, 2014.

[22] "NPS-HPC," Naval Postgraduate School, 14 April 2016. [Online] Available: https://wiki.nps.edu/pages/viewpage.action?title=Home&spaceKey=HPC. Accessed 17 April 2016.

.

[23] B. Andrus, “CUF_Week1 Introduction to hamming,” 04 April 2016. [Online] Available:https://wiki.nps.edu/display/HPC/Cluster+Users+Forum. Accessed 17 April 2016.

[24] V. Mali and S. Dange, “LearnCax,” July 25 2014. [Online]. Available: https://www.learncax.com/knowledge-base/blog/by-category/cfd/basics-of-y-plus-boundary-layer-and-wall-function-in-turbulent-flows. Accessed 9 May 2016.

[25] “Aerospace engineering,” 31 March 2012. [Online]. Available: http://aerospaceengineeringblog.com/bio-mimetic-drag-reduction-2/. Accessed 10 May 2016.

[26] Y. A. Cengel and J. M. Cimbala, *Fluids Mechanics Fundamentals Applications*, New York, NY: McGraw Hill, 2006, pp. 579–599.

[27] T. V. Karman, *Aerodynamics: Selected Topics in the light of their historical development*, Mineola, NY: Dover Publications, Inc., 2004, pp. 5–9, 62.

[28] H. Reichmann, *Cross-Country Soaring*, Santa Monica, CA: Thomson Publications, 1978, pp. 95–106.

THIS PAGE INTENTIONALLY LEFT BLANK

INITIAL DISTRIBUTION LIST

1. Defense Technical Information Center
   Ft. Belvoir, Virginia

2. Dudley Knox Library
   Naval Postgraduate School
   Monterey, California